

Computational Analysis of Carreau Nanofluid with EMHD over Stretching and Inclined Cylinder



By
Faiza Zahid

A thesis
submitted in partial fulfillment of the
requirements for the degree of
Master of Science
in
Mathematics

Supervised by
Dr. Muhammad Asif Farooq

Department of Mathematics
School of Natural Sciences
National University of Sciences and Technology
H-12, Islamabad, Pakistan

2023

THESIS ACCEPTANCE CERTIFICATE

Certified that final copy of MS thesis written by Faiza Zahid (Registration No. 00000365223), of School of Natural Sciences has been vetted by undersigned, found complete in all respects as per NUST statutes/regulations, is free of plagiarism, errors, and mistakes and is accepted as partial fulfillment for award of MS/M.Phil degree. It is further certified that necessary amendments as pointed out by GEC members and external examiner of the scholar have also been incorporated in the said thesis.


Signature: 

Name of Supervisor: Dr. Muhammad Asif Farooq

Date: 04-09-2023

Signature (HoD): 

Date: 4/9/2023

Signature (Dean/Principal): 

Date: 05.09.2023

National University of Sciences & Technology**MS THESIS WORK**

We hereby recommend that the dissertation prepared under our supervision by: "**Faiza Zahid**" Regn No. **00000365223** Titled: "**Computational Analysis of Carreau Fluid with EMHD over an Inclined and Stretching Cylinder**" accepted in partial fulfillment of the requirements for the award of **MS** degree.

Examination Committee Members1. Name: PROF. MUJEEB UR REHMANSignature: 2. Name: PROF. MERAJ MUSTAFA HASHMISignature: Supervisor's Name: Dr. MUHAMMAD ASIF FAROOQSignature: 


Head of Department

4/9/2023
Date

COUNTERSIGNEDDate: 05.09.2023


Dean/Principal

Dedicated
to my beloved
Parents and
my Sisters

Acknowledgement

First of all I would like to thank Allah Almighty, the creator of everything, for blessing me and giving me the strength and confidence to accomplish this work. I would like to convey my heartfelt thanks to my supervisor, **Dr. Muhammad Asif Farooq**, for his constant support, inspiration, helpful counselling, and invaluable assistance during my thesis. His unwavering commitment to perfection kept me focused. His nice and dedicated behaviour as well as his enthusiastic support was a source of inspiration for me to complete this thesis. My sincere gratitude is to my GEC members, **Dr. Meraj Mustafa Hashmi** and **Dr. Rizwan Ul Haq** for their guidance and support that helped me in completing this thesis on time. My heartiest and most sincere salutation to my parents and my sisters for their patience, great efforts, support, and encouragement during this time period. I would extend my gratitude to my friends **Shehneer Khan**, and **Badar-e-Alam** for their corporation and guidance on various stages during my research work. I would also like to thank my sisters **Rabia Zahid**, **Aimna Zahid**, **Zeenat Zahid** for their moral support and prayers. Lastly, I would like to acknowledge the administration staff as well as the helpers at my department for helping me whenever I needed their assistance.

Abstract

The thesis mainly discusses the behavior of Carreau nanofluid flow under MHD in a permeable medium and chemical reaction in the context of a stretching cylinder. Moreover, we discuss the influence of chemical reactions and variable thermal conductivity on EMHD Carreau nanofluid slip flow over an inclined cylinder in a porous medium. The problem is governed by a set of partial differential equations (PDEs). Similarity variables are used to convert the PDEs into a system of ordinary differential equations (ODEs). The ODEs are then solved using the *bvp4c* solver in MATLAB. The effects of several factors, including the magnetic parameter (M), Biot number (Bi) and other parameters that affect temperature, velocity, concentration, motile microorganism profiles, heat transfer coefficients (local Nusselt number and skin friction coefficient), local Sherwood number and local density of motile microorganisms are investigated. Numerical results are obtained in tabular form, which are later compared with existing research in the literature. Graphical illustrations are provided to visualize the varying effects of relevant parameters in the presence of non-Newtonian effects.

Contents

1	Introduction	1
1.1	Fluid	1
1.2	Newtonian Fluid	1
1.3	Non-Newtonian Fluid	2
1.4	Compressible Flow	2
1.5	Incompressible Flow	3
1.6	Steady Flow	3
1.7	Unsteady Flow	3
1.8	One-Dimensional Flow	3
1.9	Two-Dimensional Flow	4
1.10	Three-Dimensional Flow	4
1.11	MHD Flow	4
1.12	Carreau Fluid Model	5
1.13	Boundary Layer	6
1.13.1	Momentum Boundary Layer	7
1.13.2	Thermal Boundary Layer	7
1.13.3	Concentration Boundary layer	7
1.14	Conservation Laws	8

1.14.1	Mass Conservation Law	8
1.14.2	Momentum Conservation Law	8
1.14.3	Energy Conservation Law	9
1.15	Fourier’s law of heat conduction	9
1.16	Fick’s laws	10
1.16.1	Fick’s First Law:	10
1.16.2	Fick’s Second Law	10
1.17	Dimensionless Parameters	11
1.17.1	Magnetic Parameter (M)	11
1.17.2	Weissenberg Number	11
1.17.3	Prandtl Number (Pr)	11
1.17.4	Peclet Number (Pe)	12
1.17.5	Biot Number (Bi)	12
1.17.6	Lewis Number (Le)	12
1.17.7	Reynolds Number (Re)	13
1.18	Heat Transfer	13
1.18.1	Conduction	13
1.18.2	Convection	14
1.18.3	Radiation	14
1.19	Numerical Method	14
1.19.1	<i>bvp4c</i>	14
1.20	Literature Review	15

2	Investigation of the behavior of Carreau nanofluid flow under MHD in a permeable medium and chemical reaction in the context of a stretching cylinder	19
2.1	Mathematical Modelling	19
2.2	Measurable Properties	23
2.2.1	Skin Friction Coefficient	23
2.2.2	Local Nusselt Number	24
2.2.3	Local Sherwood Number	24
2.2.4	Local Density of Motile Microorganisms	25
2.3	Numerical Approach	25
2.4	Analysis of Results and Discussion	27
3	Analysis of EMHD Carreau Nanofluid slip flow over an inclined cylinder with chemical reaction, variable thermal conductivity	41
3.1	Mathematical Formulation	41
3.2	Physical Properties	45
3.2.1	Skin Friction Coefficient	45
3.2.2	Local Nusselt Number	45
3.2.3	Local Sherwood Number	46
3.2.4	Local Density Of Motile Microorganisms	46
3.3	Numerical Approach	47
3.4	Result and Discussion	48
3.4.1	Discussion of Tables	48
3.4.2	Discussion of Graphs	52
4	Conclusion	66

List of Figures

1.1	Boundary layer flow	8
2.1	Problem Geometry	20
2.2	The temperature dependence on Nt	33
2.3	The concentration dependence on Nt	33
2.4	The velocity dependence on α^*	34
2.5	The temperature dependence on α^*	34
2.6	The concentration dependence on α^*	35
2.7	The motile microorganisms dependence on α^*	35
2.8	The velocity dependence on Kp	36
2.9	The velocity dependence on M	36
2.10	The temperature dependence on Bi	37
2.11	The temperature dependence on Pr	37
2.12	The temperature dependence on Rd	38
2.13	The concentration dependence on γ_r	38
2.14	The concentration dependence on Sc	39
2.15	The concentration dependence on Nb	39
2.16	The motile microorganisms dependence on Sb	40
2.17	The motile microorganisms dependence on Pe	40

3.1	Problem Geometry	42
3.2	The velocity dependence on ξ	49
3.3	The temperature dependence on ξ	49
3.4	The concentration dependence on ξ	50
3.5	The motile microorganisms dependence on ξ	50
3.6	The temperature dependence on Nt	51
3.7	The concentration dependence on Nt	51
3.8	The velocity dependence on Kp	58
3.9	The velocity dependence on M	58
3.10	The velocity dependence on T_i	59
3.11	The velocity dependence on T_c	59
3.12	The temperature dependence on Bi	60
3.13	The temperature dependence on Rd	60
3.14	The temperature dependence on Pr	61
3.15	The concentration dependence on γ_r	61
3.16	The concentration dependence on Sc	62
3.17	The concentration dependence on Nb	62
3.18	The motile microorganism dependence on Sb	63
3.19	Effect of We on skin friction coefficient.	63
3.20	Effect of h_1 on on skin friction coefficient.	64
3.21	Effect of T_i on skin friction coefficient.	64
3.22	Effect of Bi on local Nusselt number.	65
3.23	Effect of Pr on local Nusselt number.	65

List of Tables

2.1	Examining the comparison of $\frac{C_f Re_x^{-\frac{1}{2}}}{2}$ under different values of M while considering the values $We = G = Kp = h_1 = 0, n = 1$	27
2.2	Considering the consequences of numerous factors regarding the coefficient of skin friction when $Nt = 0.5, Q = 0.2, Rd = 0.8, Sc = E = 0.2, \delta = 0.5, \gamma_r = 0.8, m = 1.3, Nb = 0.4, Sb = Pe = \delta_1 = 0.2, Bi = 2, Pr = 7$	28
2.3	Evaluating the consequences of numerous factors affecting the local Nusselt index when $We = M = Kp = 0.1, n = 0.5, E = Sc = 0.2, \delta = 0.5, \gamma_r = 0.8, Sb = \delta_1 = Pe = 0.2, m = 1.3$	29
2.4	Evaluating the consequences of numerous factors affecting the local Sherwood index when $n = 0.5, We = M = Kp = 0.1, Bi = 0.3, Pr = 7, Q = Sb = \delta_1 = Pe = 0.2, Rd = 0.1$	30
2.5	Impact of various factors on the motile microorganisms by taking into consideration when $n = Nt = \delta = 0.5, M = Kp = We = 0.1, Nb = 0.4, Sc = E = Q = m = 0.2, Bi = Rd = 0, Pr = 7, \gamma_r = 0.4$	31
3.1	During the examination of how $\frac{C_f(Re_x)^{-\frac{1}{2}}}{2}$ changes with different values of ξ , we take into account the following parameter values: $We = G = M = Kp = h_1 = T_t = T_C = 0$ and $n = 1$	52

3.2	Considering the consequences of numerous factors regarding the coefficient of skin friction $\varepsilon = 0.1, Nt = 0.1, Q = 0.1, Rd = 0.8, Sc = E = 0.2, \delta = 0.2, \gamma_r = 0.8, \gamma = \pi/4, m = 1.3, Nb = 0.1, Sb = 0.5, Pe = \delta_1 = 0.2, Bi = 0.3, Pr = 7$	53
3.3	Evaluating the consequences of numerous factors affecting the Nusselt index $We = M = 0.2, Kp = 0.1, n = 0.5, G = 0.1, h_1 = 0.1, T_t = T_c = 0.1, \gamma = \pi/3, E = 0.2, Sc = 0.1, \delta = \gamma_r = 0.8, Sb = \delta_1 = Pe = 0.2, m = 1.3$	54
3.4	Evaluating the consequences of numerous factors affecting the Sherwood index $We = M = 0.2, Kp = 0.1, n = 0.5, G = 0, h_1 = 0.1, T_t = T_c = 0.1, \gamma = \frac{\pi}{3}, \varepsilon = 0.3, Bi = 0.5, Pr = 7, Q = 0.1, \delta_1 = 0.8, Sb = Pe = 0.2, Rd = 0.3$	55
3.5	Impact of various factors on the motile microorganisms by taking into consideration $We = Kp = We = 0.1, n = 0.5, G = 0, h_1 = 0.1, T_i = W_r = S_b = 0.1, J = \pi/3, \varepsilon = 0.3, Nt = 0.2, Q = 0.1, Rd = 0.3, Sc = 0.1, E = 0.2, \delta = 0.2, \gamma_r = 0.8, m = 1.3, Nb = 0.4, Bi = 0.3, Pr = 7$	56

Chapter 1

Introduction

This chapter includes some fundamental definitions and preliminaries. Boundary layer flow and some associated dimensionless numbers used in this thesis are explained. The mathematical formulation for steady flow caused by axial stretching of a cylinder is discussed. The numerical procedure adopted in the problems is also explained.

1.1 Fluid

Solid, liquid and gas are three fundamental states in which a substance can exist. Anything in liquid or gas state is fluid. The distinction between the fluid and solid lies in the reaction to applied shear stress. A solid can resist the applied shear stress by static deformation whereas the fluid will result in motion regardless of how small the shear stress is. Fluid flow problems comes in a wide and different range. To make it easier fluid flow problems are categorized based on common characteristics.

1.2 Newtonian Fluid

Regardless of the shear forces applied to the fluid layers, the viscosity of these fluids remains constant. At constant temperature, the viscosity does not change. Examples

are water, milk and so on. Newton's law is represented by the equation:

$$\tau = \mu \frac{du}{dy}. \quad (1.1)$$

1.3 Non-Newtonian Fluid

Non-Newtonian fluids are characterized as fluids in which the relationship between shear stress and shear rate is not linear. For such reason, the viscosity of non-Newtonian fluids changes with the deformation rate. The relation between shear stress and shear rate in non-Newtonian fluids can be well-explained by the power law model:

$$\tau = \lambda \left(\frac{du}{dy} \right)^n, \quad (1.2)$$

where, flow behavior index is denoted by n and λ designates consistency index. Broad existence of non-Newtonian behavior in various industrial applications is obvious. Examples of non-Newtonian fluids are custard, toothpaste, honey, blood and paint etc. Fluids that are shear-thinning or pseudoplastic have a decreasing apparent viscosity with increasing shear rate. These fluids include blood, certain paints, polymer solutions, and others. Shear thickening fluids or dilatants are those whose apparent viscosity rises with shear rate. Mixture of water and cornstarch is an example of shear-thickening fluid.

1.4 Compressible Flow

Fluid flow which exhibit density variations with respect to space variables or time are treated as compressible. Flow of gases is generally regarded as compressible. Mathematically it represents as:

$$\frac{D\rho}{Dt} \neq 0. \quad (1.3)$$

1.5 Incompressible Flow

Incompressible flows are those flows where the fluid density remains consistent throughout the flow field. Most liquids are treated as incompressible fluids. Mathematically it represents as:

$$\frac{D\rho}{Dt} = 0. \quad (1.4)$$

1.6 Steady Flow

In steady flows, all the physical quantities (such as density, velocity, acceleration etc.) do not vary with time. Mathematically, for any quantity ω , one has:

$$\frac{\partial\omega}{\partial t} = 0, \quad (1.5)$$

for any physical quantity ω .

1.7 Unsteady Flow

In unsteady flow, at least any one of the fluid properties is time dependent.

$$\frac{\partial\omega}{\partial t} \neq 0, \quad (1.6)$$

for any physical quantity ω .

1.8 One-Dimensional Flow

If the flow parameter such as velocity is a function of one space coordinate only then the flow is called one-dimensional flow. Mathematically it is written as:

$$u = u(x), \quad v = 0, \quad w = 0. \quad (1.7)$$

1.9 Two-Dimensional Flow

In two-dimensional flow, the velocity field is a function of two space coordinates. Mathematically it is written as:

$$u = u(x, y), \quad v = (x, y), \quad w = 0. \quad (1.8)$$

1.10 Three-Dimensional Flow

A flow is said to be three-dimensional when the velocity is a function of three space coordinates. Mathematically it is written as:

$$u = u(x, y), \quad v = (x, y), \quad w = (x, y). \quad (1.9)$$

1.11 MHD Flow

Electric fields are induced in a conducting fluid when it moves in a magnetic field, and electric currents flow. These currents are subjected to magnetic field forces, which can significantly modify the flow. In turn, the magnetic field is modified by these currents. We interact with the magnetic and fluid-dynamic phenomena in a complex way, and flow should be examined by comparing field and fluid dynamic equations. And a wide range of physical objects, from fluid metals to cosmic plasmas, cover magnetohydrodynamic applications [25].

Combining Maxwell's equation and motion equations yields a set of equations that defines MHD flow.

$$\rho \frac{D\vec{V}}{Dt} = \vec{\nabla} \cdot \tau + (\vec{J} \times \vec{B}), \quad (1.10)$$

where \vec{V} is the velocity vector, magnetic field is expressed as \vec{B} , and \vec{J} is representing current density.

Total magnetic field is

$$B = B + B_i , \quad (1.11)$$

where B_i represents induced magnetic field.

From Ohm's Law

$$\vec{J} = \sigma \left(\vec{E} + \vec{V} \times \vec{B} \right) , \quad (1.12)$$

where E is electrical field and σ is electrical conductivity. Lorentz force is given by

$$\vec{V} \times \vec{B} = B_*^2 u \hat{i}, \quad (1.13)$$

$$\vec{J} \times \vec{B} = -\sigma B_*^2 u \hat{i}. \quad (1.14)$$

Putting (1.14) into (1.10)

$$\rho \frac{D\vec{V}}{Dt} = \vec{\nabla} \cdot \tau - \sigma B_*^2 u \hat{i}. \quad (1.15)$$

1.12 Carreau Fluid Model

In 1972, P. J. Carreau [1] suggested the Carreau fluid model. The Carreau fluid model is an extension of the power-law fluid model, which assumes a power-law relationship between shear stress and shear rate. The Carreau model introduces a more refined formulation that considers the exponential decay of viscosity with increasing shear rate, allowing it to better fit experimental data for various non-Newtonian fluids. This model relates apparent viscosity with shear rate as defined below:

$$\eta = \eta_\infty + (\eta_0 - \eta_\infty) \left[1 + (\lambda \dot{\gamma})^2 \right]^{\frac{n-1}{2}} . \quad (1.16)$$

The Carreau fundamental model is a rheological approach that characterizes the viscosity of many fluid flows, including polymer solutions, in a significant range of the magnitude of deformation rate Bird et al. [2]. A study on the heat and flow behavior of Carreau fluid in the annular space between two concentric cylinders was conducted in Khellaf and Lauriat [4]. The Carreau fluid model is often employed in industries and applications where non-Newtonian fluids are encountered, such as: polymer processing, food, beverage industry, oil, gas, pharmaceuticals, cosmetics.

1.13 Boundary Layer

In 1904, Prandtl showed that it is possible to study viscous flows by dividing them into two regions: a region that has a thin layer of flow nearby a solid wall, which is called a boundary layer that does not neglect viscous forces and an outer region that can ignore friction [26]. There are few assumptions considered for boundary layer. They are explained for continuity equation and momentum equation for two dimensional steady and incompressible flow. The velocity vector is defined as:

$$\vec{v} = u(x, y)\hat{i} + v(x, y)\hat{j} . \quad (1.17)$$

The continuity and momentum equations are:

$$u_x + v_y = 0, \quad (1.18)$$

$$x - \text{direction} \quad \rho(uu_x + vv_y) = -P_x + \mu(u_{xx} + v_{yy}), \quad (1.19)$$

$$y - \text{direction} \quad \rho(uv_x + vv_y) = -P_y + \mu(v_{xx} + v_{yy}), \quad (1.20)$$

the assumptions are:

$$u \gg v \quad \frac{\partial}{\partial y} \gg \frac{\partial}{\partial x}, \quad (1.21)$$

the resulting equations are:

$$\begin{aligned}\rho (uu_x + vv_y) &= -P_x + \mu u_{yy} , \\ -P_y &= 0.\end{aligned}\tag{1.22}$$

1.13.1 Momentum Boundary Layer

To comply with the no slip condition, the fluid particles at the solid surface exhibit the zero velocity. Subsequently, they effect the velocity of fluid particles of adjacent layer and as result they further effect the velocity of adjacent fluid particles and so on. This process of slowing of velocity takes place at a certain distance from a flat surface. Fluid velocity in the boundary layer varies from 0 to $0.99U_\infty$, where free stream velocity is exhibited by U_∞ .

1.13.2 Thermal Boundary Layer

Consider the fluid flow over a heated surface that has higher temperature than the fluid. Consequently, the region of the fluid being heated by the surface is restricted to a thin layer near the surface and this region where the temperature field exists is called thermal boundary layer. Subsequently, when we move away from the heated surface, the temperature of the fluid drops until it becomes equal to that of free stream.

1.13.3 Concentration Boundary layer

The boundary area when the concentration of nanofluid becomes closer to 99% of concentration of free stream.

The pictorial representation is given below and it is sourced from internet.

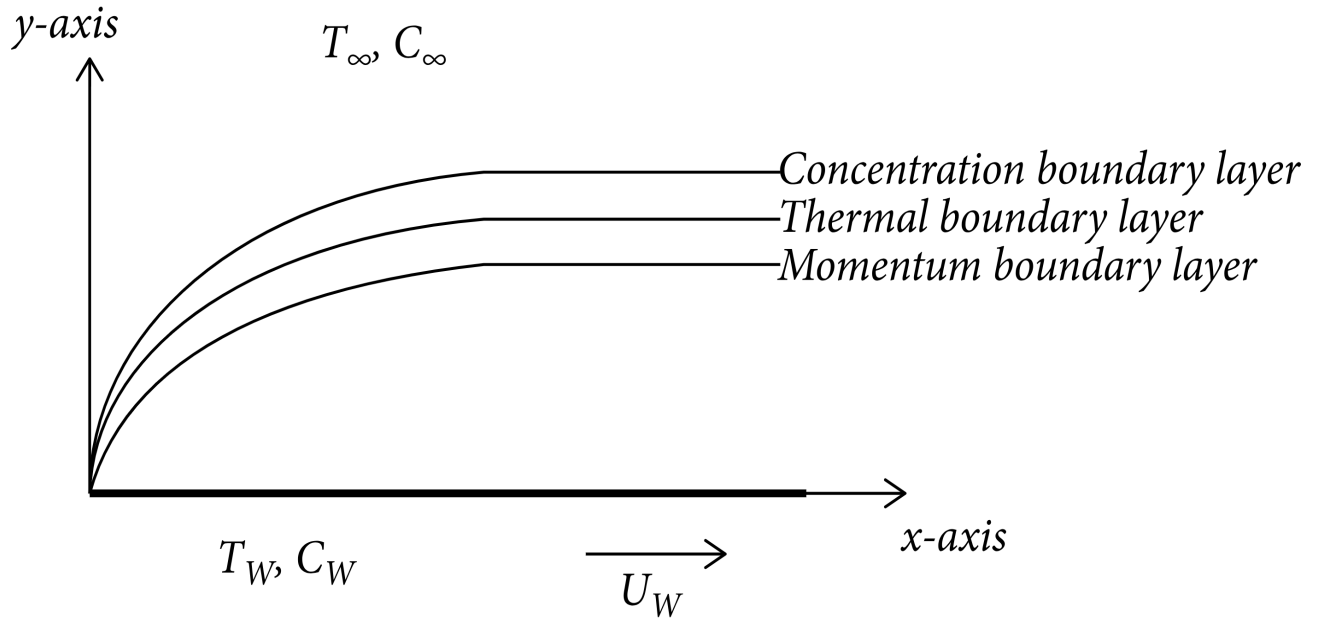


Figure 1.1: Boundary layer flow

1.14 Conservation Laws

1.14.1 Mass Conservation Law

The law states that mass can neither be created nor destroyed. The differential form for mass conservation is given by:

$$\frac{\partial \rho}{\partial t} + \vec{\nabla} \cdot (\rho \vec{V}) = 0, \quad (1.23)$$

known as continuity equation. The equation of continuity is reduced to following equation if flow is incompressible [27].

$$\vec{\nabla} \cdot \vec{V} = 0, \quad (1.24)$$

1.14.2 Momentum Conservation Law

Newton's second law $\sum \vec{F} = m\vec{a}$, is the basis upon which the law of conservation of momentum is based upon. The rate of change in momentum of a body is equal to the

force applied to it, according to the rule, and it happens in the same direction as the force. The conservation states that the momentum of system remains constant if no external force is applied.

$$\rho \frac{d\vec{V}}{dt} = -\vec{\nabla} p + \vec{\nabla} \cdot \tau + \rho \vec{g}, \quad (1.25)$$

where τ denotes the stress tensor and $\frac{d}{dt}$ represents the material time derivative.

1.14.3 Energy Conservation Law

Energy of the system remains constant although the form of the energy within a system is changed as it cannot be created or destroyed.

$$\rho C_p \frac{dT}{dt} = \vec{\nabla} \cdot (\kappa \vec{\nabla} T) + \phi, \quad (1.26)$$

where κ is the thermal conductivity, T is temperature, ϕ is the viscous dissipation function.

1.15 Fourier's law of heat conduction

It states that the heat flux (q) through a solid material is directly proportional to the negative gradient of temperature ($\vec{\nabla} T$) and the material's thermal conductivity (κ):

$$\vec{q} = -\kappa(\vec{\nabla} T). \quad (1.27)$$

\vec{q} is the heat flux vector (the amount of heat energy transferred per unit area per unit time), κ is the thermal conductivity of the material, and $\vec{\nabla} T$ is the temperature gradient vector (the rate of change of temperature with respect to distance in a specific direction).

1.16 Fick's laws

Fick's laws are a set of fundamental equations in fluid mechanics that describe the diffusion of substances, such as particles, atoms, or molecules, in a medium. They were formulated by Adolf Fick, a German physiologist, in the mid-19th century. Fick's laws are essential in understanding mass transport processes in various scientific and engineering disciplines.

1.16.1 Fick's First Law:

This law describes the steady-state diffusion of a substance through a homogeneous medium. It states that the rate of diffusion (J) of a substance is proportional to the negative gradient of its concentration (C) with respect to distance (x). Mathematically, Fick's first law can be expressed as:

$$J = -D \frac{\partial C}{\partial x}, \quad (1.28)$$

where J is the diffusive flux (the amount of substance diffusing per unit area per unit time), D is the diffusion coefficient (also known as the diffusivity) of the substance in the medium and $\frac{\partial C}{\partial x}$ is the concentration gradient (the rate of change of concentration with respect to distance).

Fick's first law is applicable when the concentration gradient is constant over time and there is no net accumulation or depletion of the diffusing substance in the medium.

1.16.2 Fick's Second Law

This law describes the time-dependent diffusion of a substance in a medium. It considers changes in concentration with respect to both time and distance. Fick's second law is a partial differential equation and is expressed as:

$$\frac{\partial C}{\partial T} = D \frac{\partial^2 C}{\partial x^2}. \quad (1.29)$$

1.17 Dimensionless Parameters

1.17.1 Magnetic Parameter (M)

The ratio of Lorentz force to inertial force is the magnetic interaction parameter.

$$M = \frac{\sigma B_*^2}{\rho a}, \quad (1.30)$$

where B_* is the magnetic field strength, σ is the electrical conductivity, ρ is the density and a is the positive constant.

1.17.2 Weissenberg Number

The Weissenberg number indicates the ratio of the time scale of elastic effects to the time scale of viscous effects in the fluid.

$$We = \frac{t_r}{t_f}, \quad (1.31)$$

where t_f is time-scale of a flow and t_r represent relaxation time. it is a measure of the fluid's ability to resist deformation and return to its original shape after being deformed. A high Weissenberg number indicates a strong elastic response and the potential for complex behavior such as shear-thickening or shear-thinning, depending on the specific properties of the fluid.

1.17.3 Prandtl Number (Pr)

Prandtl number is expressed as the ratio between momentum diffusivity to thermal diffusivity.

$$Pr = \frac{\nu}{\alpha} = \frac{c_p \mu}{\kappa}, \quad (1.32)$$

where κ and c_p are the thermal conductivity and the specific heat respectively.

1.17.4 Peclet Number (Pe)

The Peclet number represents the ratio between rate of convection to the diffusion rate in the convection and diffusion transport system.

$$Pe = \frac{\text{Convective transport rate}}{\text{Diffusive transport rate}} = \frac{Ul}{D}. \quad (1.33)$$

U the characteristic flow velocity, l is the characteristic length scale of the system, and D is the diffusion coefficient.

1.17.5 Biot Number (Bi)

It represents the ratio between the resistance offered to heat transfer by the inside of the body to the external resistance.

$$Bi = \frac{\text{Internal conductive resistance}}{\text{External convective resistance}} = \frac{hl}{\kappa_{eff}}. \quad (1.34)$$

h is the convective heat transfer coefficient at the surface of the solid, l is the characteristic length (usually the thickness) of the solid material, κ_{eff} is the effective thermal conductivity

1.17.6 Lewis Number (Le)

The ratio between the thermal diffusion to the mass diffusion is represented by the Schmidt number . It characterizes the fluid flows where the simultaneous occurrence of heat and mass transfer happens. Thus, it explains the relative thickness of thermal and concentration boundary layers.

$$Le = \frac{\text{Thermal diffusivity}}{\text{Mass diffusivity}} = \frac{\alpha}{D}, \quad (1.35)$$

where α is given thermal diffusivity and D is mass diffusivity.

1.17.7 Reynolds Number (Re)

The Reynolds number refer to the ratio between inertial and viscous forces.

$$Re = \frac{\rho u L}{\mu}, \quad (1.36)$$

where L shows characteristic length, u denotes the velocity of flow. Reynolds number is used to classify laminar and turbulent flow situations of fluid. Viscous forces are dominant at low Reynolds numbers ($Re < 2000$), this causes laminar flow. Inertial force becomes relatively dominant at a high Reynolds number ($Re > 4000$) creating turbulence in the fluid flow.

1.18 Heat Transfer

Heat transfer takes places between physical systems as a result of temperature gradient. Flow of heat occurs from a region of higher temperature to a region lower temperature. The three modes of heat transfer are conduction, convection and radiation.

1.18.1 Conduction

Conduction is a process of heat transfer which occurs due to the collision of molecules in a medium. As a result of Molecules with higher kinetic energy colliding with molecules having lower kinetic energy, lower kinetic energy molecules obtain energy. Hence, energy transfer in conduction is due to interaction of molecules in a medium. This conduction is also known as heat conduction. Heat conduction, electrical conduction, and sound conduction are all terms that are frequently used to describe three different types of activity. Heat conduction rely on the temperature gradient, cross section area of material and physical properties. The rate of conduction is calculated as follows:

$$Q = \frac{k A(T_{hot} - T_{cold})}{d} \quad (1.37)$$

in which k represents thermal conductivity, A is the area, d denotes thickness of body, T_{hot} and T_{cold} are temperatures of hot region and cold regions respectively.

1.18.2 Convection

Convection is defined as the flow of fluid molecules from higher to lower thermal energy regions. Heat convection takes place due the density difference of fluid molecules in the region. As the temperature increases volume of fluid molecules also increases, hence the density of molecules decreases. This causes displacement of molecules. The three types of convection are Natural (free) convection, Forced convection and mixed convection. Newton's law of cooling has given Heat Transfer Mechanism as below:

$$Q = h A(T_w - T_f), \quad (1.38)$$

Where h denotes heat transfer coefficient. T_w is the wall temperature and T_f is surrounding temperature.

1.18.3 Radiation

In the infrared and visible regions of the electromagnetic spectrum, radiation is the transmission of thermal energy carried by photons of light. Radiation is a mechanism by which all bodies constantly emit thermal energy. It can be sent without the use of any medium.

1.19 Numerical Method

1.19.1 *bvp4c*

The *bvp4c* solver in MATLAB is an effective tool to solve fairly complex problems. For solving nonlinear systems of equations, the algorithm uses an iteration structure. It is based on collocation method. The residual of the continuous solution is used for

mesh selection and error control. As *bvp4c* is an iterative method, the algorithm's effectiveness will ultimately be determined by the ability to make an initial guess for the solution. The MATLAB commands used are:

$$soll = bvp4c((odefun, bcfun, solinit), \quad (1.39)$$

where *odefun* is the function of system of first order differential equations, *bcfun* indicates the boundary conditions under consideration and *solinit* forms the initial guess for the boundary value problem.

1.20 Literature Review

The relationship between shear stress and shear rate is non-linear in non-Newtonian fluids. These fluids are of significant importance in various industrial and manufacturing techniques, such as insulating materials, extrusion, hot rolling, glass-fiber manufacture, metal spinning and metal extrusion. To interpret non-Newtonian dynamics, different fluid models such as the Casson, Williamson, viscoelastic, and tangent hyperbolic models are used. The Carreau model is a fundamental modeling technique that demonstrates power-law behavior. It was proposed by Carreau [1] in 1972 as a four-parameter approach that represents generalized Newtonian fluid models. The Carreau fluid is a distinct model that characterizes power-law fluids and retrieves Newtonian fluid as a limiting case [2, 3]. The viscosity of a generalized Newtonian fluid is permitted to change in proportion to the amount of the deformation rate. They rotated the inner cylinder while keeping the outer cylinder stationary and found that the friction coefficient of the rotating cylinder decreased due to the influence of shear thinning. Akber et al. [5] proposed a hypothesis on the boundary layer stagnation point flow of Carreau fluid approaching a porous medium and stretching surface. They noticed that as the elastic parameter increased, the skin friction coefficient slightly increased.

In reference [6, 7, 8] different researchers employed various techniques to study fluids using different media.

Nanofluids are a type of fluid that contains small particles or fibers called nanoparticles or nanofibers, respectively, suspended in a base fluid, such as glycol, oil, and water. These particles are typically between 1 to 100 nanometers in size and can modify the mechanical and thermal properties of the fluid. One of the key benefits of nanofluids is their increased thermal conductivity, which can improve heat transfer in various applications, such as nuclear reactors, heat exchangers, and electronics cooling.

The field of nanotechnology has attracted significant interest from researchers due to the potential benefits offered by nanomaterials, including increased thermal conductivity. Nanotechnology has uses in diverse fields, such as industrial, bio-medical and engineering, including power generation, transportation, air conditioning, and nuclear system cooling. Nanofluids have gained attention due to their suitable viscosity, enhanced stability, and better wetting properties. Research centers have been established worldwide to facilitate the development of nanofluids. Previously, it was believed that achieving higher thermal conductivity in fluids would require substantial pumping power, making it impractical for various applications. However, Choi and Eastman [9] proposed a theory that nanoparticles could develop efficient thermal conductivity instead of relying on high pumping power to improve heat transfer.

Buongiorno [10] has discovered that both thermophoresis and Brownian motion are essential mechanisms for increasing the thermal conductivity of nanofluids, which has significant implications in various scientific fields, such as power generation, cooling systems in vehicles, coolant processing, and biomedical applications such as cancer

diagnosis. The thermal conductivity of these fluids is crucial in determining the coefficient of heat transfer between the heat source and sheet.

This approach was employed by Khan and Pop [11] in examining the boundary layer flow over a stretched sheet. According to their findings, the Nusselt number decreases as values of thermophoresis, Prandtl number, and Brownian motion increase, while the opposite is true for the Sherwood number. In a related study, Noghrehabadi et al. [12] provided a succinct summary of slip boundary conditions and nanofluids, revealing that an increase in the slip parameter results in a reduction of the momentum boundary layer and an increase in the thermal boundary layer. Rohni et al. [13] employed the Buongiorno model to examine the unsteady flow of nanofluid over a shrinking sheet with convective heat transfer. Their study revealed the presence of non-unique solutions for specific parameters. Malvandi et al. [14] a researchers investigated the behavior of a nanofluid over a stretching sheet using convective boundary conditions. Khan et al. [15] conducted research on the melting phenomenon of Carreau nanofluid in the existence of heat occupation in an unsteady wedge flow. Their findings showed that an increase in melting parameters resulted in a decrease in nanoparticle temperature distribution and concentration. K. L. Hsiao [16] utilized the Carreau nanofluid and a parameter control technique to enhance the activation energy system.

Magnetohydrodynamics (MHD) has gained significant interest due to its broad range of applications in fields such as petroleum, environmental technology, and chemical engineering. MHD involves the application of a magnetic field perpendicular to the direction of the flow of liquid, creating a drag force called Lorentz force that opposes the direction of fluid motion. The study of the behavior of electrically conductive fluids, such as plasma and liquid metals, in the presence of magnetic fields, is referred to

as MHD. Industrial applications of MHD include liquid metal blankets for fusion reactors, crystal growth, and metal casting, among others. Vajravelu and Hadjinicolaou [17] examined heat transfer resulting from convection over a stretching surface in the presence of an applied magnetic field, while Nazar et al. [18] investigated heat transfer and flow of hydromagnetic fluid over a vertically stretched sheet. In both studies, it was observed that the local heat flux at the wall and skin friction decreased as the magnetic parameter increased. In their research, Ganesh et al. [19] investigated the axisymmetric slip flow of an MHD Newtonian fluid on a vertically stretching cylinder. They found that while skin friction coefficient increased with slip and surface convection parameters, it decreased with magnetic parameter.

Chapter 2

Investigation of the behavior of Carreau nanofluid flow under MHD in a permeable medium and chemical reaction in the context of a stretching cylinder

In this chapter, we discuss the extension work that is motivated by Song et al. [20] that explores the implications of convection, with an emphasis on thermal radiation and chemical reaction for a flow of a Carreau nanofluid over a stretching cylinder considering a permeable medium.

2.1 Mathematical Modelling

Take into account a two-dimensional, steady and incompressible Carreau nanofluid within a porous medium along a horizontally stretching cylinder. The magnetic field effect B_* is perpendicular to the direction of fluid flow. The cylindrical axis is measured along the x -axis and the r -axis is measured radially as shown in Fig.2.1. The Cauchy stress tensor for a Carreau fluid is calculated using [21]:

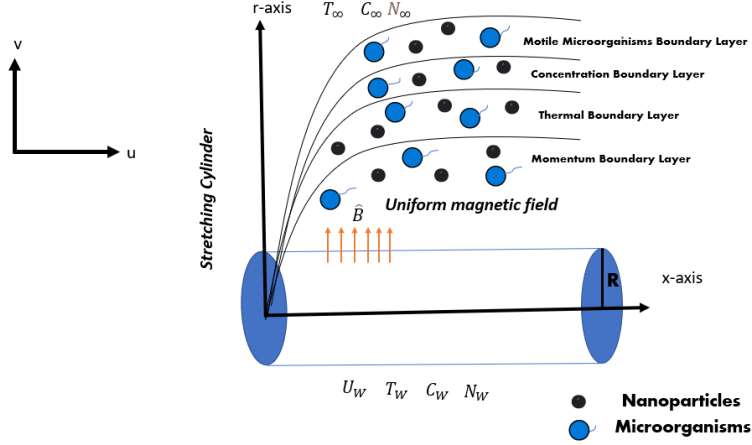


Figure 2.1: Problem Geometry

$$\vec{\tau} = \hat{\mu} \hat{A}, \quad (2.1)$$

and

$$\frac{\hat{\mu} - \hat{\mu}_\infty}{\hat{\mu}_0 - \hat{\mu}_\infty} = [1 + (\Gamma \check{\gamma})^2]^{\frac{n-1}{2}}, \quad (2.2)$$

where $\hat{\mu}_0$ is zero shear-rate viscosity, $\hat{\mu}_\infty$ is the infinite shear-rate viscosity, $\hat{\mu}$ is shear-rate viscosity, \hat{A} is the first kind Rivlin-Erickson tensor, Γ is a constant named material time.

$$\hat{A} = \nabla V + (\nabla V)^T, \quad (2.3)$$

$$\check{\gamma} = \sqrt{\frac{1}{2} \sum_i \sum_j \check{\gamma}_{ij} \check{\gamma}_{ij}} = \sqrt{\frac{1}{2} \text{II}} = \sqrt{\frac{1}{2} \text{tr}(\hat{A}^2)}, \quad (2.4)$$

Here, II represents the second invariant of the strain tensor. The study considers $\check{\eta}_\infty = 0$ and $\Gamma \check{\gamma} < 1$ as assumptions. By utilizing binomial expansion, equation (2.2) can be characterized as follows:

$$\hat{\mu} = \hat{\mu}_0 \left[1 + \frac{n-1}{2} (\Gamma \check{\gamma})^2 \right]. \quad (2.5)$$

The equation (2.1) can be redefined as:

$$\ddot{\tau} = \dot{\mu}_\circ \left[1 + \frac{n-1}{2} (\Gamma\check{\gamma})^2 \right] \dot{A}. \quad (2.6)$$

The boundary layer approximation of the momentum equation, continuity equation, energy equation, concentration equation and motile microorganisms equation is written as [21, 22]:

$$\frac{\partial(ru)}{\partial x} + \frac{\partial(rv)}{\partial r} = 0, \quad (2.7)$$

$$u \frac{\partial u}{\partial x} + v \frac{\partial u}{\partial r} = \nu \left(\frac{\partial^2 u}{\partial r^2} + \frac{1}{r} \frac{\partial u}{\partial r} + \frac{3\Gamma^2(n-1)}{2} \left(\frac{\partial u}{\partial r} \right)^2 \frac{\partial^2 u}{\partial r^2} + \frac{\Gamma^2(n-1)}{2r} \left(\frac{\partial u}{\partial r} \right)^3 \right) - \frac{\sigma \hat{B}^2}{\rho} u - \frac{\nu}{\kappa_1} u, \quad (2.8)$$

$$u \frac{\partial T}{\partial x} + v \frac{\partial T}{\partial r} = \alpha \frac{\partial^2 T}{\partial r^2} + \frac{\alpha}{r} \frac{\partial T}{\partial r} + \frac{(\rho C)_p}{(\rho C_p)_f} \left(D_B \frac{\partial C}{\partial r} \frac{\partial T}{\partial r} + \frac{D_T}{T_\infty} \left(\frac{\partial T}{\partial r} \right)^2 \right) - \frac{1}{(\rho C_p)_f} \frac{\partial}{\partial r} (r q_r) + \frac{Q^*(T - T_\infty)}{\rho C_p}, \quad (2.9)$$

$$u \frac{\partial C}{\partial x} + v \frac{\partial C}{\partial r} = D_B \frac{\partial^2 C}{\partial r^2} + \frac{D_B}{r} \frac{\partial C}{\partial r} + \frac{D_T}{T_\infty r} \frac{\partial T}{\partial r} + \frac{D_T}{T_\infty} \frac{\partial^2 T}{\partial r^2} - \kappa_r^* (C - C_\infty) \left(\frac{T}{T_\infty} \right)^m \exp \left(\frac{-E_a}{\kappa_b T_\infty} \right), \quad (2.10)$$

$$u \frac{\partial N}{\partial x} + v \frac{\partial N}{\partial r} + \frac{bW_C}{(C_w - C_\infty)} \left[\frac{\partial}{\partial r} \left(N \frac{\partial C}{\partial r} \right) \right] = \frac{D_m}{r} \frac{\partial}{\partial r} \left(r \frac{\partial N}{\partial r} \right). \quad (2.11)$$

The system under consideration involves the following variables: velocity components (u and v), kinematic viscosity (ν), power law index (n), porosity (κ_1), electrical conductivity (σ), fluid density (ρ), ambient temperature (T_∞), temperature (T), thermal conductivity (α), specific heat (C_p), thermal radiation (q_r), heat source (Q^*), concentration (C), the concentration at the wall (C_w), ambient concentration (C_∞), concentration of microorganisms (N), the concentration of microorganisms at the wall (N_w), ambient concentration of microorganisms (N_∞), chemical reaction rate (κ_r^*), fitted rate constant (m), Brownian diffusion (D_B), thermophoretic diffusion D_T , microorganism diffusivity (D_m), swimming speed of maximum cell (W_C) and chemotaxis constant (b).

The thermal radiation is approximated by the Rosseland model as:

$$q_r = - \frac{16\sigma^* T_\infty^3}{3\kappa^*} \frac{\partial T}{\partial r}$$

here σ^* is Stefan-Boltzmann constant and κ^* is the mean absorption coefficient.

The boundary conditions under consideration are expressed as follows:

$$u = u_w = \frac{ax}{L}, \quad -k \frac{\partial T}{\partial r} + q_r = h_f(T_f - T), \quad v = 0, \quad D_B \frac{\partial C}{\partial r} + \frac{D_T}{T_\infty} \frac{\partial T}{\partial r} = 0, \\ N = N_w \quad \text{at} \quad r = R, \tag{2.12}$$

$$u \rightarrow 0, \quad T \rightarrow T_\infty, \quad C \rightarrow C_\infty, \quad N \rightarrow N_\infty, \quad \text{as} \quad r \rightarrow \infty. \tag{2.13}$$

The similarity variable and similarity transformations are given below:

$$\beta = \sqrt{\frac{a}{l\nu}} \left(\frac{r^2 - R^2}{2R} \right), \quad \Psi(\beta) = \sqrt{\frac{\nu a}{l}} x R f(\beta), \quad u = \frac{1}{r} \frac{\partial \Psi}{\partial r}, \quad v = -\frac{1}{r} \frac{\partial \Psi}{\partial x}, \tag{2.14}$$

$$\theta(\beta) = \frac{T - T_\infty}{T_f - T_\infty}, \quad \chi(\beta) = \frac{N - N_\infty}{N_w - N_\infty}, \quad \phi(\beta) = \frac{C - C_\infty}{C_w - C_\infty}. \tag{2.15}$$

$$(1 + 2\alpha^* \beta) f'''' + 2\alpha^* f'' + \frac{3(n-1)}{2} We^2 (1 + 2\alpha^* \beta) (f'')^2 \left((1 + 2\alpha^* \beta) f''''(\beta) + \alpha^* f''(\beta) \right) + \\ \frac{(n-1)}{2} We^2 (1 + 2\alpha^* \beta) \alpha^* (f''(\beta))^3 - (f'(\beta))^2 + f(\beta) f''(\beta) - M^2 f'(\beta) - K_p f'(\beta) = 0, \tag{2.16}$$

$$(1 + 2\alpha^* \beta) \theta'' + 2\alpha^* \theta' + \frac{4}{3} Rd \left((1 + 2\alpha^* \beta) \theta'' + 2\alpha^* \theta' \right) + (1 + 2\alpha^* \beta) \\ Pr \left(Nt(\theta')^2 + Nb\theta' \phi' \right) + (f\theta' + Q\theta) Pr = 0, \tag{2.17}$$

$$(1 + 2\alpha^* \beta) \phi'' + 2\alpha^* \phi' + Scf\phi' + \frac{Nt}{Nb} \left(2\alpha^* \theta' + (1 + 2\alpha^* \beta) \theta'' \right) - Sc\gamma_r \\ (1 + \delta\theta)^m \phi \exp \left(\frac{-E}{(1 + \delta\theta)} \right) = 0, \tag{2.18}$$

$$(1 + 2\alpha^* \beta) \chi'' + 2\alpha^* \chi' + Sbf\chi' - Pe \left((1 + 2\alpha^* \beta) (\phi' \chi' + (\chi + \delta_1) \phi'') + (\chi + \delta_1) \alpha^* \phi' \right) = 0, \tag{2.19}$$

with boundary conditions:

$$\begin{aligned}
f(0) &= 0, \quad f'(0) = 1, \quad f'(\infty) = 0, \\
\theta'(0) &= -\frac{Bi(1 - \theta(0))}{1 + \frac{4}{3}Rd}, \quad \theta(\infty) = 0, \\
Nb\phi'(0) + Nt\theta'(0) &= 0, \quad \phi(\infty) = 0, \\
\chi(0) &= 1, \quad \chi(\infty) = 0,
\end{aligned} \tag{2.20}$$

$\alpha^* = \frac{1}{R}\sqrt{\frac{\nu l}{a}}$ is curvature parameter, $M^2 = \frac{\sigma \hat{B}^2 l}{\rho a}$ is magnetic parameter, $Nb = \frac{\tau D_B (C_w - C_\infty)}{\nu C_\infty}$ is Brownian parameter, $Q = \frac{l Q^*}{\rho a C_p}$ is heat generation parameter, $K_p = \frac{\nu l}{\kappa_1 a}$ is porosity parameter, $We^2 = \frac{\Gamma^2 x^2 a^3}{\nu l^3}$ is Weissenberg number, $Nt = \frac{\tau D_T (T_f - T_\infty)}{\nu T_\infty}$ is thermophoresis constant, $\gamma_r = \frac{\kappa_r^* l}{a}$ denotes chemical reaction parameter, $Pr = \frac{\nu}{\alpha}$ denotes Prandtl number, $Sc = \frac{\nu}{D_B}$ is the Schmidt number, $Sb = \frac{\nu}{D_m}$ is the bioconvection Schmidt number, $E = \frac{-E_a}{\kappa_b T_\infty}$ is activation energy, $Rd = \frac{4\sigma^* T_\infty^3}{\kappa^* \kappa}$ denotes the radiation parameter, $Pe = \frac{bW_c}{D_m}$ denotes the Peclet number, $Bi = \frac{h_f}{k} \sqrt{\frac{\nu l}{a}}$ denotes the Biot number, $\delta = \frac{T_f - T_\infty}{T_\infty}$ denotes temperature difference, $\delta_1 = \frac{N_w}{N_w - N_\infty}$ denotes the microorganism difference parameter.

2.2 Measurable Properties

2.2.1 Skin Friction Coefficient

The C_f is a dimensionless factor that defines frictional drag on a surface. It is characterized as follows:

$$C_f = \frac{\tau_w''}{\frac{1}{2}\rho u_w^2}. \tag{2.21}$$

The shear stress at the wall is denoted as:

$$\tau_w'' = \hat{\mu} \left(\frac{\partial u}{\partial r} + \frac{\Gamma^2 (n-1)}{2} \left(\frac{\partial u}{\partial r} \right)^3 \right)_{r=R}. \tag{2.22}$$

After applying equation (2.22) in equation (2.21), we obtain:

$$\frac{C_f Re_x^{-\frac{1}{2}}}{2} = f''(0) + \frac{(n-1)}{2} We^2 \left(f''(0) \right)^3. \quad (2.23)$$

Here, the local Reynolds number is defined as: $Re_x = \frac{u_w x}{\nu}$.

2.2.2 Local Nusselt Number

We evaluate local Nusselt number (Nu_x) at surface to analyse heat transfer rate at surface.

$$Nu_x = -\frac{x \dot{q}_w}{\kappa(T_f - T_\infty)}. \quad (2.24)$$

Fourier's law at the wall is determined as:

$$\dot{q}_w = \kappa \left(\frac{\partial T}{\partial r} \right)_{r=R} + q_r. \quad (2.25)$$

Using equation (2.25) in equation(2.24) we get:

$$Nu_x Re_x^{-\frac{1}{2}} = -\left(1 + \frac{4}{3} Rd\right) \theta'. \quad (2.26)$$

2.2.3 Local Sherwood Number

The local Sherwood number (Sh_x) is s calculated as follows:

$$Sh_x = \frac{x j_w^*}{D_B(C_W - C_\infty)}. \quad (2.27)$$

By applying Fick's law, we can represent mass transfer as:

$$j_w^* = -D_B \left(\frac{\partial C}{\partial r} \right)_{r=R}. \quad (2.28)$$

Using equation (2.28) in equation (2.27) we get:

$$Sh_x Re_x^{-\frac{1}{2}} = -\phi'(0). \quad (2.29)$$

2.2.4 Local Density of Motile Microorganisms

The local density of moving microorganisms is determined by:

$$Nn_x = \frac{x i_w^*}{D_m(N_W - N_\infty)}. \quad (2.30)$$

The flux of motile surface microorganisms is expressed as follows:

$$i_w^* = -D_m \left(\frac{\partial N}{\partial r} \right)_{r=R}. \quad (2.31)$$

Using equation(2.31) in equation (2.30) we get:

$$Nn_x R e_x^{-\frac{1}{2}} = -\chi'(0). \quad (2.32)$$

2.3 Numerical Approach

Differential equations of a more complex nature and higher order are frequently used to simulate various engineering and scientific situations. In the contemporary literature, numerous mathematical approaches are available to be implemented in computing simulations. With regard to its precision and efficiency, dimensionless observations (2.16)–(2.19) and boundary conditions (2.20) are arithmetically addressed by utilising MATLAB computational curriculum's *bvp4c* solver. Initially, coupled nonlinear ODEs are modified into first order representations to use the given equation:

$$\begin{aligned} f &= \Omega_1, \quad f' = \Omega'_1 = \Omega_2, \quad f'' = \Omega'_2 = \Omega_3, \\ \theta &= \Omega_4, \quad \theta' = \Omega'_4 = \Omega_5, \\ \phi &= \Omega_6, \quad \phi' = \Omega_7, \\ \chi &= \Omega_8, \quad \chi' = \Omega'_8 = \Omega_9, \end{aligned} \quad (2.33)$$

$$\begin{aligned}\Omega'_3 = & \left(\frac{1}{(1 + 2\alpha^*\beta) + \frac{3(n-1)}{2}(1 + 2\alpha^*\beta)^2 We^2(\Omega_3)^2} \right) (-2\alpha^*\Omega_3 - \frac{(n-1)}{2} We^2\alpha^*(1 + 2\alpha^*\beta)(\Omega_3)^3 \\ & - \frac{3(n-1)}{2} We^2\alpha^*(1 + 2\alpha^*\beta)(\Omega_3)^3 + M^2\Omega_2 + Kp\Omega_2 + (\Omega_2)^2 - \Omega_1\Omega_3),\end{aligned}\quad (2.34)$$

$$\begin{aligned}\Omega'_5 = & \left(\frac{1}{(1 + 2\alpha^*\beta) + \frac{4}{3}(1 + 2\alpha^*\beta)Rd} \right) (-2\alpha^*\Omega_5 - Pr(1 + 2\alpha^*\beta)(Nt(\Omega_5)^2 + Nb\Omega_5\Omega_7) - \\ & Pr(Q\Omega_4 + \Omega_1\Omega_5) - \frac{4}{3}2\alpha^*Rd\Omega_5),\end{aligned}\quad (2.35)$$

$$\begin{aligned}\Omega'_7 = & \left(\frac{1}{(1 + 2\alpha^*\beta)} \right) (-2\alpha^*\Omega_7 - 2\alpha^*\frac{Nt}{Nb}\Omega_5 - (1 + 2\alpha^*\beta)\frac{Nt}{Nb}\Omega'_5 - Sc\Omega_1\Omega_7 + \\ & \gamma_r Sc(1 + \delta\Omega_4)^m \Omega_6 \exp\left(\frac{-E}{(1 + \delta\Omega_4)}\right)),\end{aligned}\quad (2.36)$$

$$\begin{aligned}\Omega'_9 = & \frac{1}{(1 + 2\alpha^*\beta)} (Pe((1 + 2\alpha^*\beta)(\Omega_7\Omega_9 + (\delta_1 + \Omega_8)\Omega'_7) + (\delta_1 + \Omega_8)\alpha^*\Omega_7) \\ & - 2\alpha^*\Omega_9 - Sb\Omega_1\Omega_9),\end{aligned}\quad (2.37)$$

$$\Omega_1(0) = 0, \quad \Omega_2(0) = 1, \quad \Omega_2(\infty) = 0, \quad (2.38)$$

$$\Omega_5(0) = -Bi(1 - \Omega_4(0)), \quad \Omega_4(\infty) = 0, \quad (2.39)$$

$$Nb\Omega_7(0) + Nt\Omega_5(0) = 0, \quad \Omega_6(\infty) = 0, \quad (2.40)$$

$$\Omega_8(\infty) = 0, \quad \Omega_8(0) = 1. \quad (2.41)$$

M	Malik et al. [23]	Bilal et al. [24]	Current Result
0.0	1.0000	1.0000	1.0000
0.5	-1.11802	-1.11800	-1.11803
1.0	-1.41419	-1.41420	-1.41421

Table 2.1: Examining the comparison of $\frac{C_f Re_x^{-\frac{1}{2}}}{2}$ under different values of M while considering the values $We = G = Kp = h_1 = 0$, $n = 1$.

2.4 Analysis of Results and Discussion

We examine the numerical outcomes of $\frac{C_f(Re)^{-\frac{1}{2}}}{2}$ for varying values of M in Table 2.1 and compare them with the published results. Table 2.2 demonstrates the effect of various factors on C_f . α^* , M and Kp illustrate the curvature, magnetic and permeability parameters respectively. The value of C_f has shown an upward trend as the values of α^* , M , and Kp have increased. However, it has a negligible effect on C_f when n is increased. While C_f is diminishing when the value of We increases. Table 2.3 emphasizes that the value of Nu_x has shown an upward trend as the values of α^* , Pr , Bi , and Nt have increased. Conversely, Nu_x diminishes when the values of Rd and Q increase. It has a negligible effect on Nu_x when Nb is increased. Table 2.4 demonstrates that the Sh_x has shown an upward trend as Nt increased while diminishing with the rise of α^* , Nb and having a negligible effect on Sh_x when γ_r , Sc , m , E and δ are increased. Table 2.5 demonstrates that the increments in the value of Nn_x as the α^* and Sb increases and then diminish as the Pe and γ_1 increases.

Thermophoresis refers to the phenomenon where the transportation of particles or

α^*	We	M	Kp	n	$-\frac{C_f Re_x^{-\frac{1}{2}}}{2}$
0.2	0.1	0.1	0.1	0.5	1.13009
0.4	-	-	-	-	1.20647
0.6	-	-	-	-	1.28161
0.2	0.3	-	-	-	1.11969
-	0.5	-	-	-	1.09691
-	0.7	-	-	-	1.05397
-	0.1	0.3	-	-	1.16878
-	-	0.5	-	-	1.24205
-	-	0.7	-	-	1.3435
-	-	0.1	0.3	-	1.2242
-	-	-	0.5	-	1.31067
-	-	-	0.7	-	1.3911
-	-	-	0.1	0.3	1.12959
-	-	-	-	0.6	1.13035
-	-	-	-	0.9	1.1311

Table 2.2: Considering the consequences of numerous factors regarding the coefficient of skin friction when $Nt = 0.5$, $Q = 0.2$, $Rd = 0.8$, $Sc = E = 0.2$, $\delta = 0.5$, $\gamma_r = 0.8$, $m = 1.3$, $Nb = 0.4$, $Sb = Pe = \delta_1 = 0.2$, $Bi = 2$, $Pr = 7$.

molecules is induced by a temperature gradient. The enhancement of thermophoresis is attributed to the temperature difference between the ambient temperature and the temperature at the surface, resulting that increasing both the fluid's temperature and concentration. The thermophoretic force acting on small particles is increased as it is influenced by the presence of a temperature gradient, which in turn leads to an enhancement of the thermophoresis parameter (Nt), shown in Fig.2.2, and Fig.2.3.

Fig.2.4 illustrates that α^* affects the velocity profile. The radius has an inverse relationship with the curvature parameter. By increasing the α^* the cylinder radius declines, thus resulting in fluid receiving less resistance which shows an upward trend in velocity distribution. Fig.2.5 elucidates how α^* affects on temperature distribution.

α^*	Nb	Pr	Q	Nt	Rd	Bi	$-\theta'(0)$
0.2	0.4	7	0.2	0.2	0.1	0.3	1.30638
0.4	-	-	-	-	-	-	1.31283
0.6	-	-	-	-	-	-	1.31862
0.2	0.4	-	-	-	-	-	1.30638
-	0.6	-	-	-	-	-	1.30638
-	0.8	-	-	-	-	-	1.30638
-	0.4	5	-	-	-	-	1.25185
-	-	6	-	-	-	-	1.28287
-	-	7	-	-	-	-	1.30638
-	-	7	0.1	-	-	-	1.33750
-	-	-	0.2	-	-	-	1.30638
-	-	-	0.3	-	-	-	1.25830
-	-	-	0.2	0.2	-	-	1.30638
-	-	-	-	0.4	-	-	1.29996
-	-	-	-	0.6	-	-	1.29257
-	-	-	-	0.2	0.1	-	1.30638
-	-	-	-	-	0.3	-	1.79597
-	-	-	-	-	0.5	-	2.34274
-	-	-	-	-	0.1	0.3	1.30638
-	-	-	-	-	-	0.5	1.33546
-	-	-	-	-	-	0.7	1.35887

Table 2.3: Evaluating the consequences of numerous factors affecting the local Nusselt index when $We = M = Kp = 0.1$, $n = 0.5$, $E = Sc = 0.2$, $\delta = 0.5$, $\gamma_r = 0.8$, $Sb = \delta_1 = Pe = 0.2$, $m = 1.3$.

α^*	Nt	Nb	γ_r	m	E	δ	Sc	$-\phi'(0)$
0.2	0.5	0.4	0.8	1.3	0.2	0.5	0.2	1.42989
0.4	-	-	-	-	-	-	-	1.43719
0.6	-	-	-	-	-	-	-	1.44378
0.2	0.5	-	-	-	-	-	-	1.42989
-	0.7	-	-	-	-	-	-	1.98955
-	0.9	-	-	-	-	-	-	2.53914
-	0.5	0.4	-	-	-	-	-	1.42989
-	-	0.6	-	-	-	-	-	0.953259
-	-	0.8	-	-	-	-	-	0.714944
-	-	0.4	0.8	-	-	-	-	1.42989
-	-	-	1.2	-	-	-	-	1.42391
-	-	-	1.4	-	-	-	-	1.42085
-	-	-	0.8	1.3	-	-	-	1.42989
-	-	-	-	1.5	-	-	-	1.42924
-	-	-	-	1.7	-	-	-	1.42856
-	-	-	-	1.3	0.2	-	-	1.42989
-	-	-	-	-	0.4	-	-	1.43157
-	-	-	-	-	0.6	-	-	1.43301
-	-	-	-	-	0.2	0.5	-	1.42989
-	-	-	-	-	-	0.7	-	1.42830
-	-	-	-	-	-	0.9	-	1.42667
-	-	-	-	-	-	0.5	0.2	1.42989
-	-	-	-	-	-	-	0.5	1.40298
-	-	-	-	-	-	-	0.7	1.38169

Table 2.4: Evaluating the consequences of numerous factors affecting the local Sherwood index when $n = 0.5$, $We = M = Kp = 0.1$, $Bi = 0.3$, $Pr = 7$, $Q = Sb = \delta_1 = Pe = 0.2$, $Rd = 0.1$.

α^*	Sb	Pe	δ_1	$-\chi'(0)$
0.2	1.3	0.3	0.7	0.208953
0.3	-	-	-	0.217799
0.4	-	-	-	0.229419
0.2	1.3	-	-	0.208953
-	1.5	-	-	0.288028
-	1.7	-	-	0.361661
-	1.3	0.1	-	0.560086
-	-	0.3	-	0.208953
-	-	0.5	-	0.135229
-	-	0.3	0.7	0.208953
-	-	-	0.8	0.148008
-	-	-	1.2	0.056590

Table 2.5: Impact of various factors on the motile microorganisms by taking into consideration when $n = Nt = \delta = 0.5$, $M = Kp = We = 0.1$, $Nb = 0.4$, $Sc = E = Q = m = 0.2$, $Bi = Rd = 0$, $Pr = 7$, $\gamma_r = 0.4$.

Surging the α^* results in an upward trend in temperature distribution. Increments in the velocity distribution boosted the motion of fluid particles which means the heat transfer rate is also boosted. Fig.2.6 elucidates that the concentration distribution dwindles when the α^* is boosted. The reason is that velocity and temperature show an upward trend, which results in changes in the fluid's viscosity, when the viscosity of fluid decreases, movement of the nanoparticles is boosted which in turn gives a decline in the concentration. Fig.2.7 portrays that the profile of the motile microorganisms is boosted when surging α^* . Because the concentration of particles is decreased, the movement of nanoparticles is boosted that is the cells move faster and they interact with each other, resulting in an upward trend in the density of motile microorganisms.

Fig.2.8 illustrates how the permeability (Kp) parameter influences the velocity profile. When increment in Kp , the resistance to the fluid's nanoparticles is boosted and velocity distribution decreases. The M affects the profile of velocity, as demonstrated in

Fig.2.9. As the magnetic field strengthens, the corresponding increment in the Lorentz force hinders the motion of fluid, leading to a decrease in velocity. Fig.2.10 depicts how the profile of temperature is affected by Bi . As increment in Bi number which turn in an upward trend in temperature distribution. Fig.2.11 depicts how the profile of temperature is affected by Pr . Increasing in Pr causes a reduction in temperature distribution. Fig.2.12 illustrates the rate of heat transmission rises with a boost in Rd . The particles within the system absorb the radiation, resulting in a temperature gradient between the surface and the top layers. Because of this, heat is transported more rapidly. Fig.2.13 depicts the influence of γ_r on the concentration distribution. Concentration distribution decreased as the increment in γ_r .

Fig.2.14 depicts how the concentration distribution is affected by Sc . Profile of concentration decreased as the increment in Sc . As the Schmidt number increases, the rate of mass transfer also increases, leading to a decrease in concentration profiles. Nb represents the relationship between the concentration gradient and momentum diffusivity. Before the intersection of the three curves, the concentration at the wall exceeds the ambient concentration. As a result, the concentration near the boundary experiences an upward surge. The motion of nanoparticles is enhanced when the temperature is increased and there is a change in kinetic energy, this causes the concentration distribution to be reduced depicted in Fig.2.15. Fig.2.16 illustrates that the presence of motile microorganisms decreases with an increase in Sb . This increase in Sb corresponds to a dwindle in the diffusivity of microorganisms, leading to a decline in their movement. Fig.2.17 illustrates the impact of the Pe on motile microorganisms distribution. When we increase Pe , results in raised in the motile microorganisms distribution.

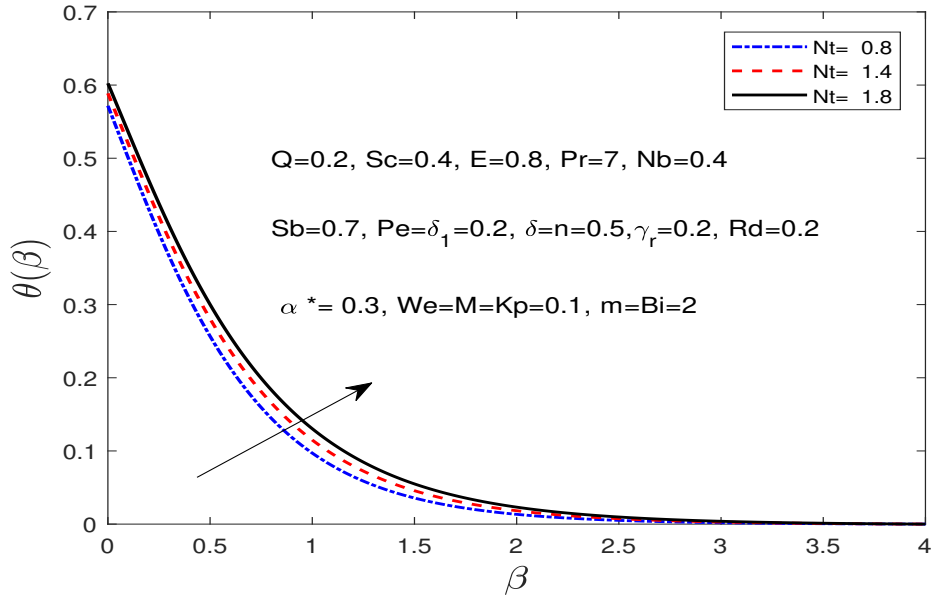


Figure 2.2: The temperature dependence on Nt .

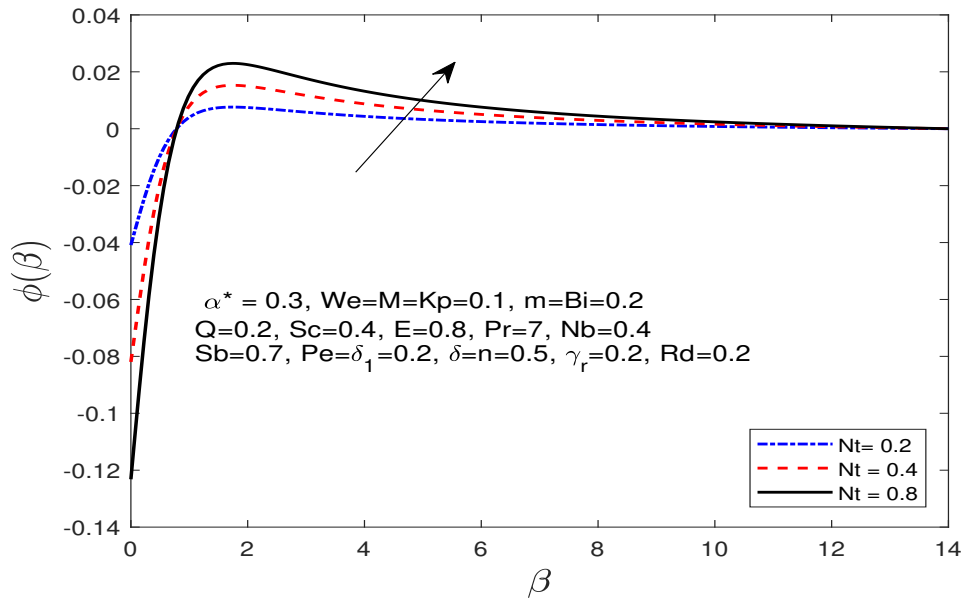


Figure 2.3: The concentration dependence on Nt .

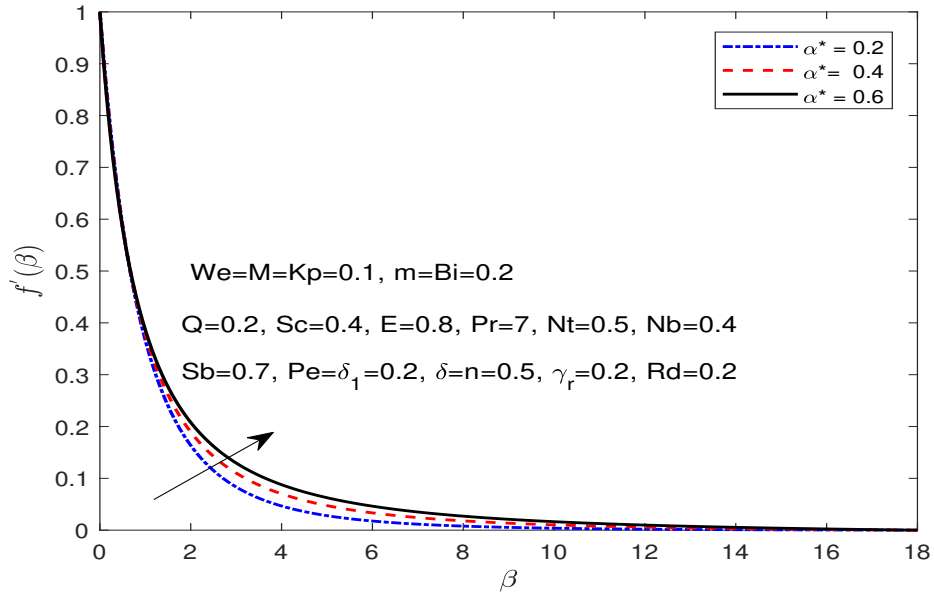


Figure 2.4: The velocity dependence on α^* .

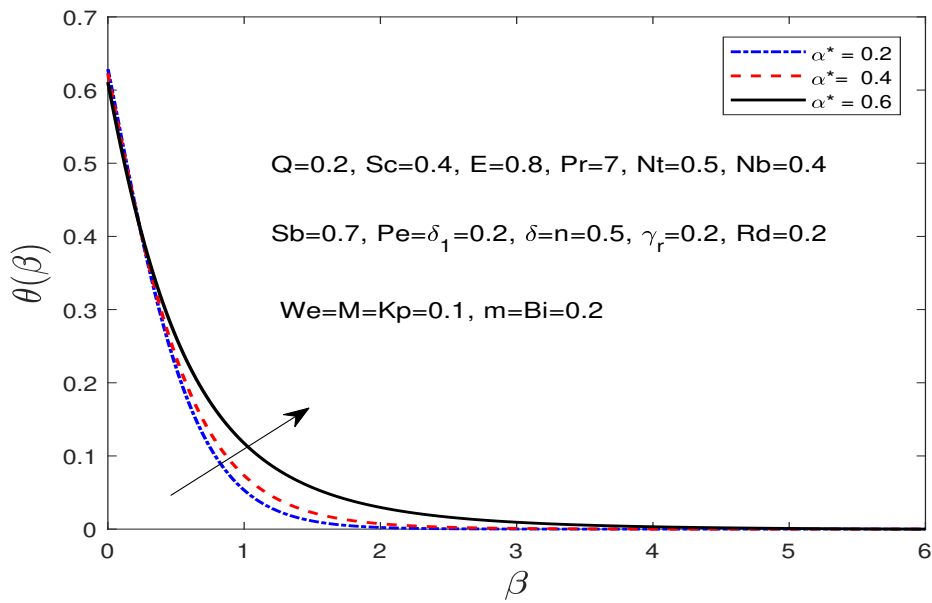


Figure 2.5: The temperature dependence on α^*

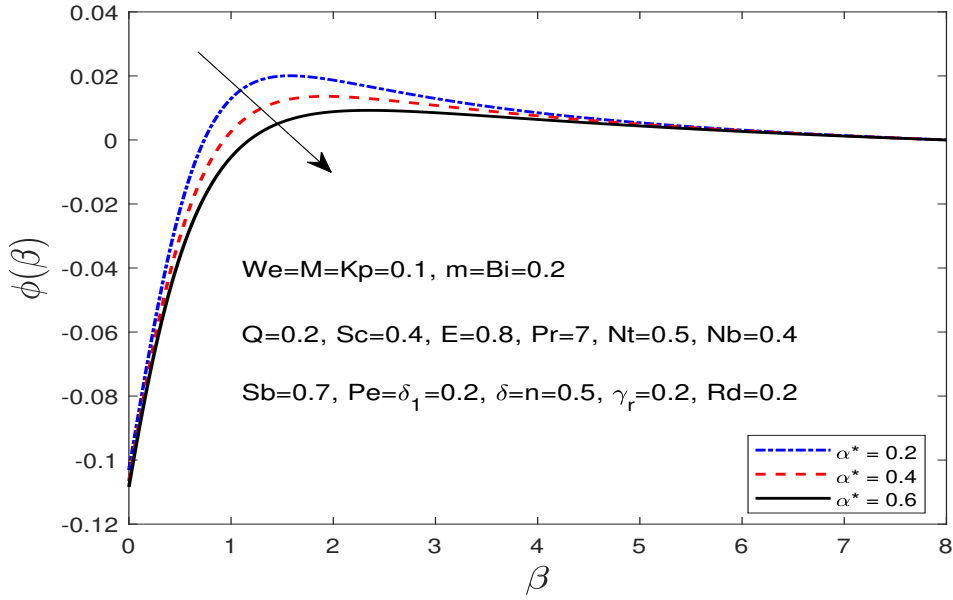


Figure 2.6: The concentration dependence on α^* .

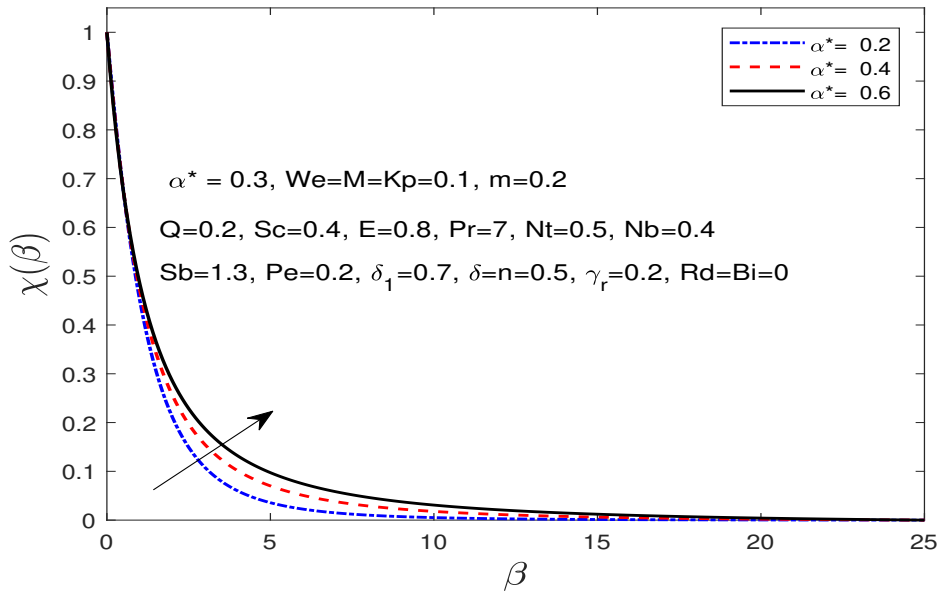


Figure 2.7: The motile microorganisms dependence on α^* .

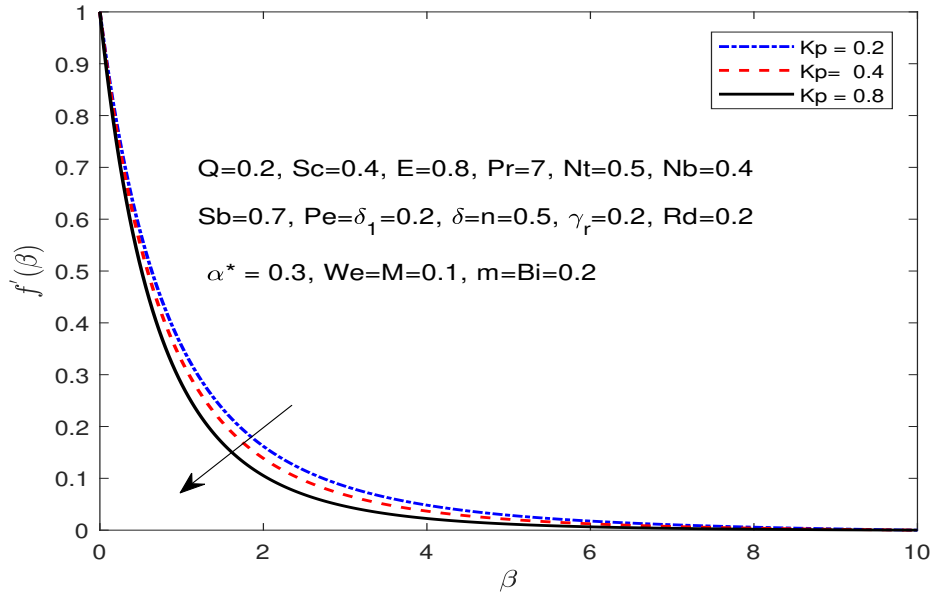


Figure 2.8: The velocity dependence on Kp .

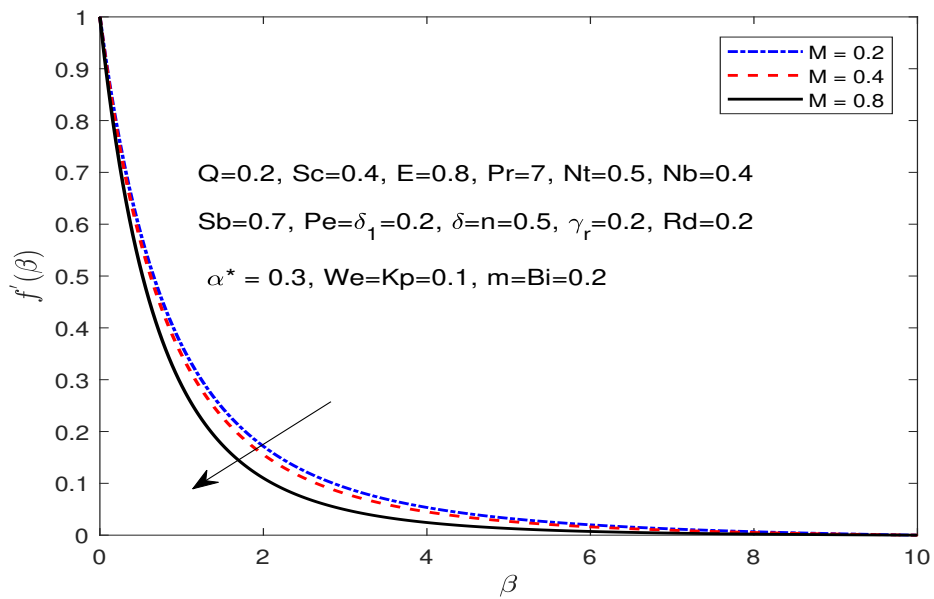


Figure 2.9: The velocity dependence on M .

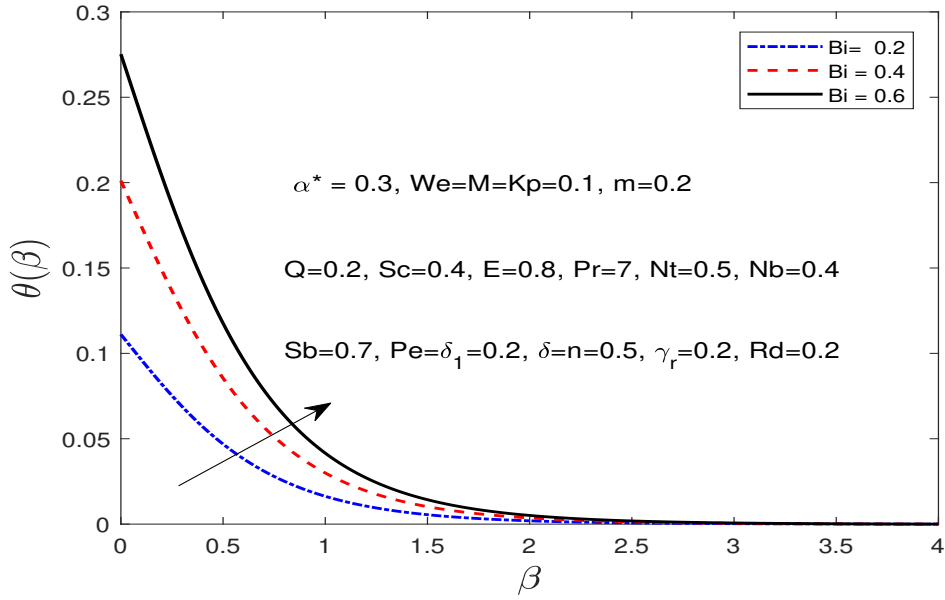


Figure 2.10: The temperature dependence on Bi .

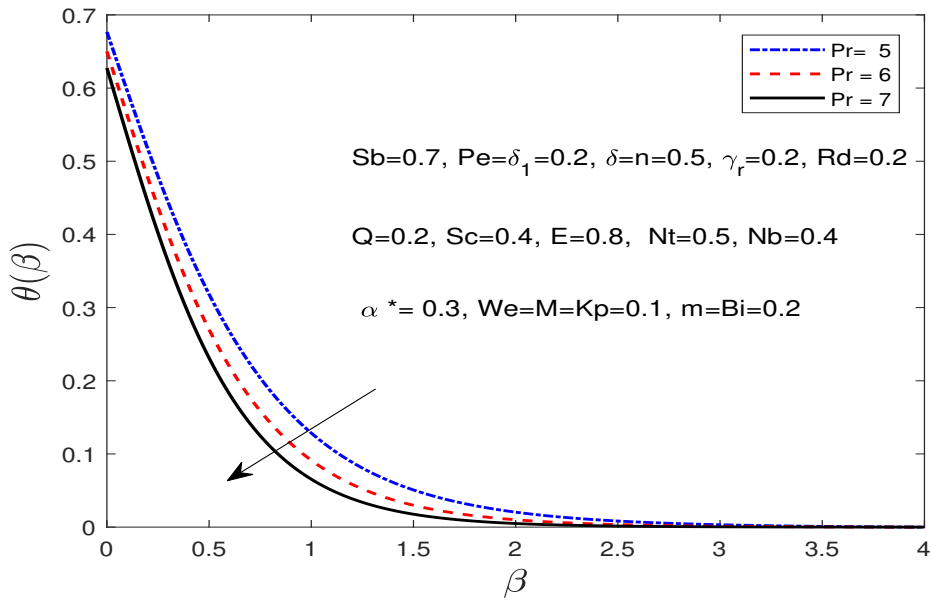


Figure 2.11: The temperature dependence on Pr .

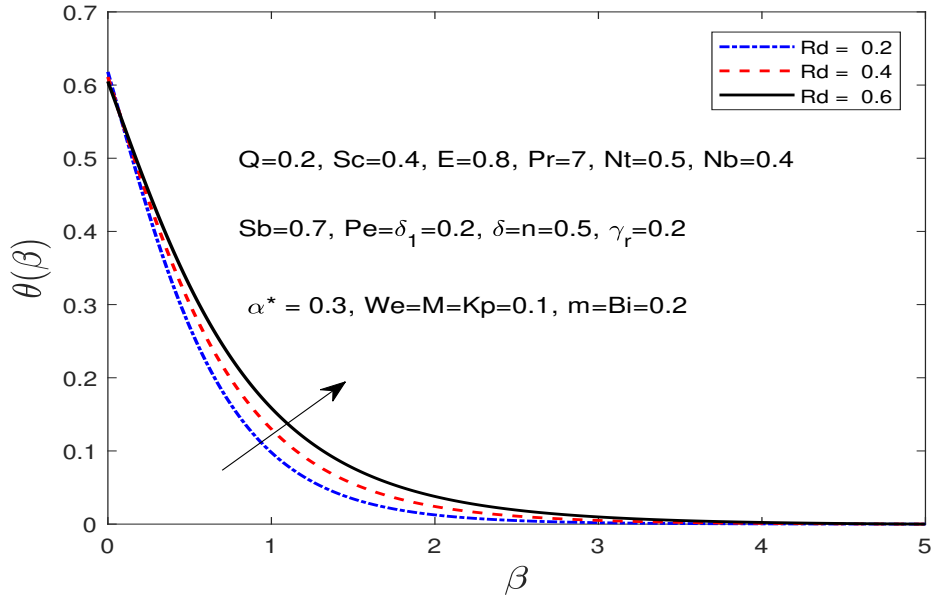


Figure 2.12: The temperature dependence on Rd .

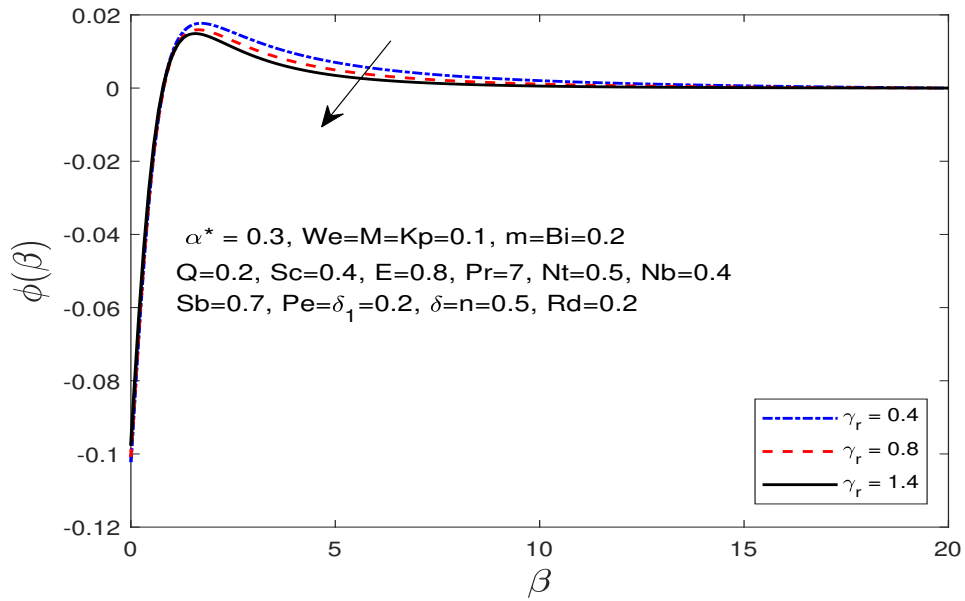


Figure 2.13: The concentration dependence on γ_r .

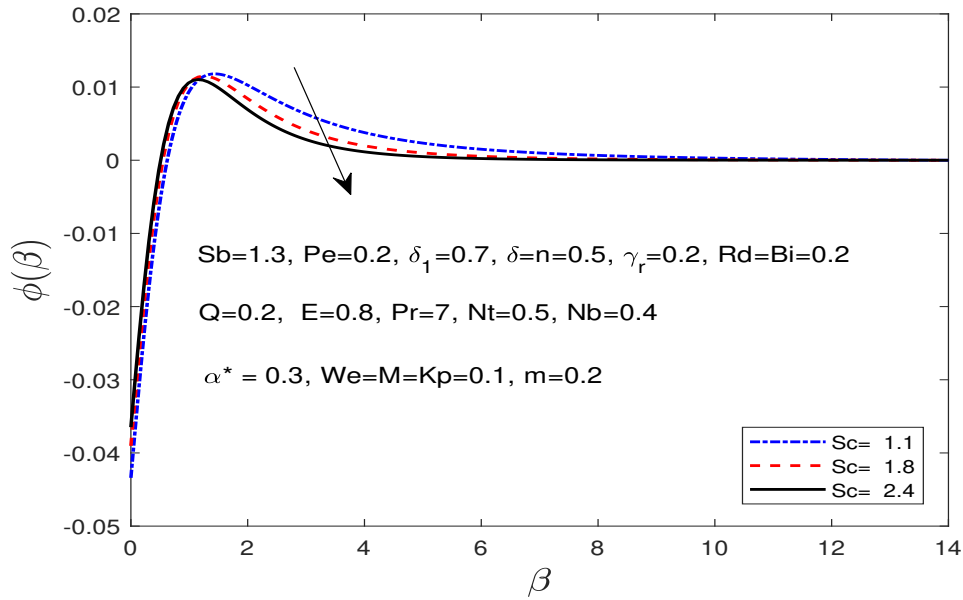


Figure 2.14: The concentration dependence on Sc .

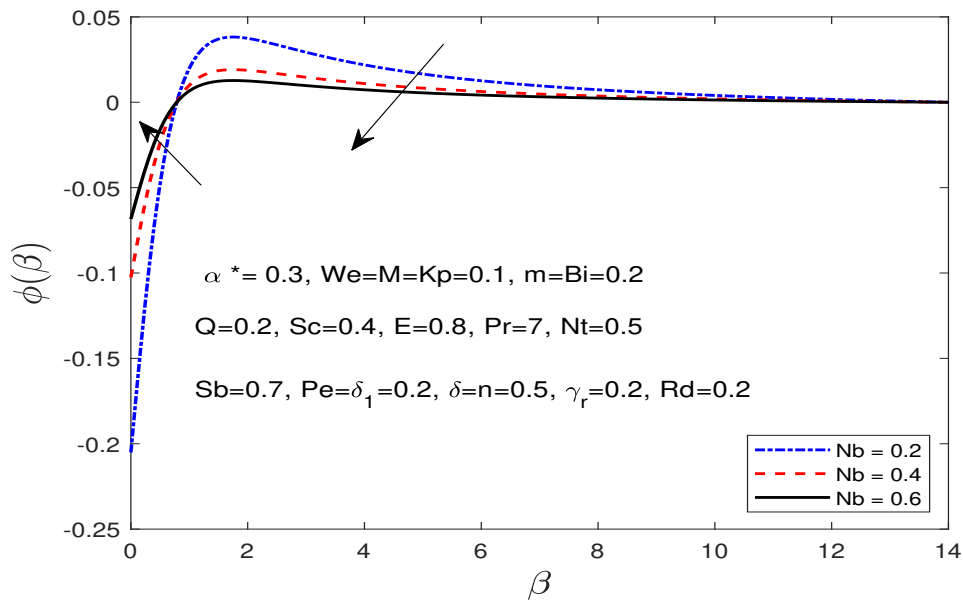


Figure 2.15: The concentration dependence on Nb .

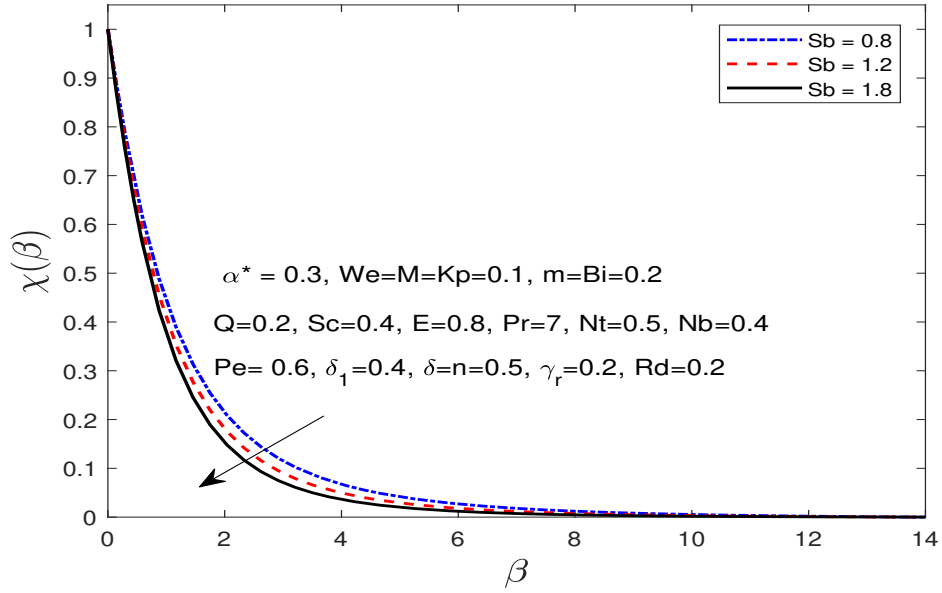


Figure 2.16: The motile microorganisms dependence on Sb .

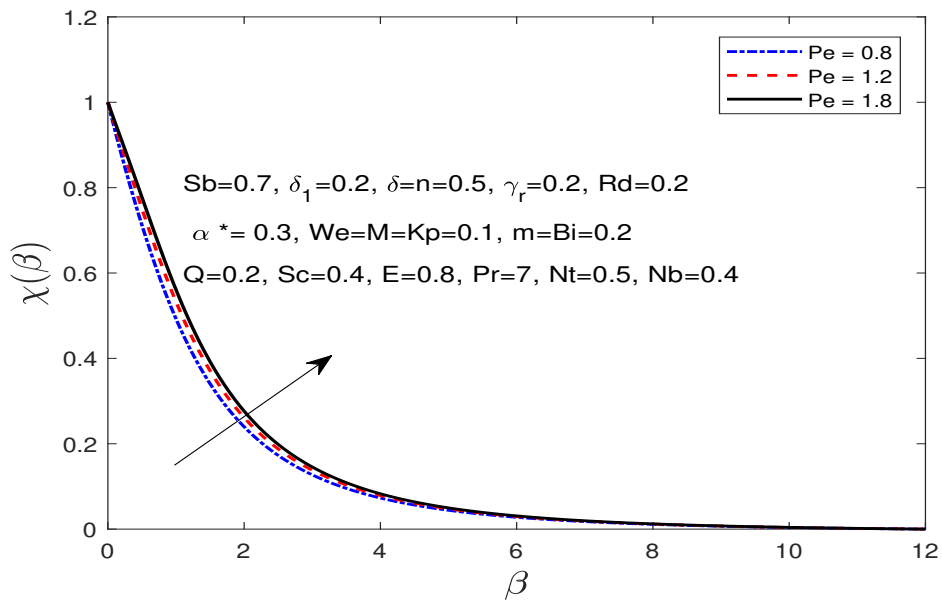


Figure 2.17: The motile microorganisms dependence on Pe .

Chapter 3

Analysis of EMHD Carreau Nanofluid slip flow over an inclined cylinder with chemical reaction, variable thermal conductivity

In this chapter, we discuss the extension work that is motivated by Waqas et al. [30] that analysis of variable EMHD Carreau Nanofluid slip flow over an inclined cylinder with chemical reaction and variable thermal conductivity.

3.1 Mathematical Formulation

We conducted a study on the two-dimensional EMHD flow of a steady laminar flow of Carreau bio-nanofluid through an inclined cylinder. The analysis considered the effects of variable thermal conductivity, slip boundary conditions and Arrhenius activation energy. At $r = 0$, the surface has been located. Both the variable magnetic field $B(x) = \frac{\hat{B}x}{l}$ and the variable electric field $E(x) = \frac{\hat{E}x}{l}$ have been applied orthogonal to the direction of fluid flow. Due to its low value, the magnetic Reynolds number does not produce a magnetic field. As seen in Fig.3.1, the cylindrical axis follows the x -axis whereas the radial direction follows the r -axis.

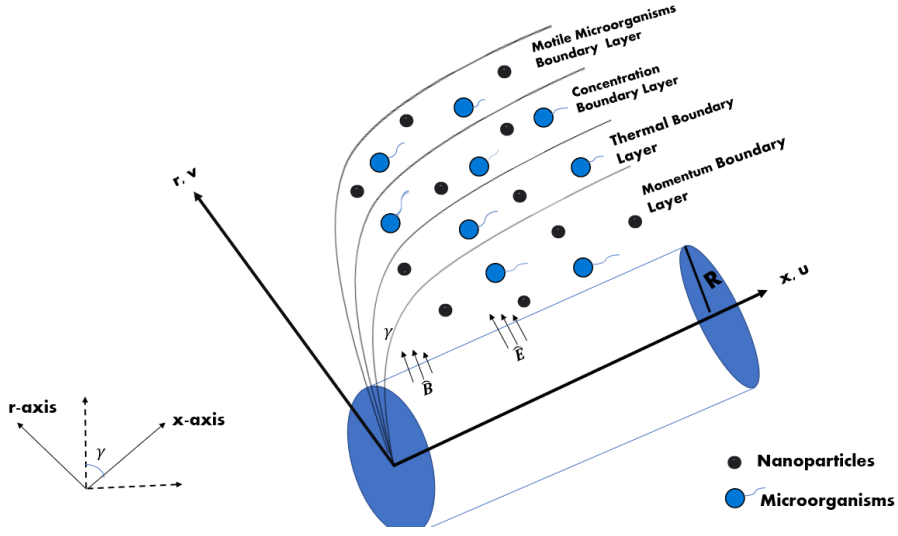


Figure 3.1: Problem Geometry

The equations for continuity, momentum, energy, continuity, concentration and motile microorganisms under the boundary layer approximation can be expressed as follows:

$$\frac{\partial(ru)}{\partial x} + \frac{\partial(rv)}{\partial r} = 0, \quad (3.1)$$

$$u \frac{\partial u}{\partial x} + v \frac{\partial u}{\partial r} = \nu \left(\frac{\partial^2 u}{\partial r^2} + \frac{1}{r} \frac{\partial u}{\partial r} + \frac{3\Gamma^2(n-1)}{2} \left(\frac{\partial u}{\partial r} \right)^2 \frac{\partial^2 u}{\partial r^2} + \frac{\Gamma^2(n-1)}{2r} \left(\frac{\partial u}{\partial r} \right)^3 \right) - g((T - T_\infty)\omega_t - \omega_c(C - C_\infty)) \cos(\gamma) - \frac{\sigma}{\rho_f} \left(\hat{B}^2(x)u - \hat{E}(x)\hat{B}(x) \right) - \frac{\nu}{\kappa_1} u, \quad (3.2)$$

$$u \frac{\partial T}{\partial x} + v \frac{\partial T}{\partial r} = \frac{1}{\rho C_p} \frac{1}{r} \left(\frac{\partial}{\partial r} \left(\kappa(T)r \frac{\partial T}{\partial r} \right) \right) + \frac{(\rho C)_p}{(\rho C)_f} \left(D_B \frac{\partial C}{\partial r} \frac{\partial T}{\partial r} + \frac{D_T}{T_\infty} \left(\frac{\partial T}{\partial r} \right)^2 \right) - \frac{1}{\rho C_p} \frac{1}{r} \frac{\partial(rq)}{\partial r} + \frac{Q^*(T - T_\infty)}{\rho C_p}, \quad (3.3)$$

$$u \frac{\partial C}{\partial x} + v \frac{\partial C}{\partial r} = D_B \frac{\partial^2 C}{\partial r^2} + \frac{D_B}{r} \frac{\partial C}{\partial r} + \frac{D_T}{T_\infty r} \frac{\partial T}{\partial r} + \frac{D_T}{T_\infty} \frac{\partial^2 T}{\partial r^2} - \kappa_r^2 (C - C_\infty) \left(\frac{T}{T_\infty} \right)^m \exp \left(\frac{-E_a}{\kappa_b T} \right), \quad (3.4)$$

$$u \frac{\partial N}{\partial x} + v \frac{\partial N}{\partial r} + \frac{bW_C}{(C_w - C_\infty)} \left[\frac{\partial}{\partial r} \left(N \frac{\partial C}{\partial r} \right) \right] = \frac{D_m}{r} \frac{\partial}{\partial r} \left(r \frac{\partial N}{\partial r} \right). \quad (3.5)$$

The system under consideration involves the following variables: velocity components (u and v), kinematic viscosity (ν), power law index (n), gravitational acceleration (g), porosity (κ)₁, electrical conductivity (σ), fluid density (ρ), ambient temperature (T_∞), temperature (T), thermal conductivity (α), specific heat (C_p), thermal radiation (q_r), heat source (Q^*), concentration (C), thermophoretic diffusion (D_T), a concentration at the wall (C_w), ambient concentration (C_∞), concentration of microorganisms (N), the concentration of microorganisms at the wall (N_w), ambient concentration of microorganisms (N_∞), chemical reaction rate (κ_r^*), fitted rate constant (m), Brownian diffusion (D_B), microorganism diffusivity (D_m), swimming speed of maximum cell (W_C) and chemotaxis constant (b). For a Carreau nanofluid, the variable thermal conductivity can be described as:

$$\kappa(T) = \kappa_\infty(1 + \epsilon\theta), \quad (3.6)$$

The specified conditions at the boundary are as follows:

$$u = u_w + u_{slip} = \frac{ax}{l} + h \frac{\partial u}{\partial r} \left(1 + \frac{n-1}{2} \Gamma^2 \left(\frac{\partial u}{\partial r} \right)^2 \right), \quad -k \frac{\partial T}{\partial y} + q_r = h_f(T_f - T), \quad v = 0, \\ D_B \frac{\partial C}{\partial r} + \frac{D_T}{T_\infty} \frac{\partial T}{\partial r} = 0, \quad N = N_w \quad \text{at} \quad r = R, \quad (3.7)$$

$$u \rightarrow 0, \quad T \rightarrow T_\infty, \quad C \rightarrow C_\infty, \quad N \rightarrow N_\infty, \quad \text{as} \quad r \rightarrow \infty. \quad (3.8)$$

The similarity variable and similarity transformations are given below:

$$\omega = \sqrt{\frac{a}{l\nu}} \left(\frac{r^2 - R^2}{2R} \right), \quad \Psi(\omega) = \sqrt{\frac{\nu a}{l}} x R f(\omega), \quad u = \frac{1}{r} \frac{\partial \Psi}{\partial r}, \quad v = -\frac{1}{r} \frac{\partial \Psi}{\partial x}, \quad (3.9)$$

$$\theta(\omega) = \frac{T - T_\infty}{T_f - T_\infty}, \quad \chi(\omega) = \frac{N - N_\infty}{N_w - N_\infty}, \quad \phi(\omega) = \frac{C - C_\infty}{C_w - C_\infty}. \quad (3.10)$$

$$\begin{aligned}
& (1 + 2\xi\omega) f'''' + 2\xi f'' + \frac{3(n-1)}{2} We^2 (1 + 2\xi\omega) (f'')^2 \left((1 + 2\xi\omega) f''''(\omega) + \xi f''(\omega) \right) + \\
& \frac{(n-1)}{2} We^2 (1 + 2\xi\omega) \xi (f''(\omega))^3 - (f'(\omega))^2 + f(\omega) f''(\omega) - M^2 \left(f'(\omega) - G \right) \\
& - K_p f'(\omega) + (T_t + T_c) \cos(\gamma) = 0, \tag{3.11}
\end{aligned}$$

$$\begin{aligned}
& (1 + 2\xi\omega) \left((1 + \varepsilon\theta) \theta'' + \varepsilon\theta'^2 \right) + (1 + \varepsilon\theta) 2\xi\theta' + (1 + 2\xi\omega) Pr \left(Nt(\theta')^2 + Nb\theta'\phi' \right) + \\
& Pr \left(f\theta' + Q\theta \right) + \frac{4}{3} Rd \left((1 + 2\xi\omega)\theta'' + \xi\theta' \right) = 0, \tag{3.12}
\end{aligned}$$

$$\begin{aligned}
& (1 + 2\xi\omega)\phi'' + 2\xi\phi' + Scf\phi' + \frac{Nt}{Nb} \left(2\xi\theta' + (1 + 2\xi\omega)\theta'' \right) \\
& - Sc\gamma_r (1 + \delta\theta)^m \phi \exp \left(\frac{-E}{(1 + \delta\theta)} \right) = 0, \tag{3.13}
\end{aligned}$$

$$(1 + 2\xi\omega) \chi'' + 2\xi\chi' + Sbf\chi' - Pe \left((1 + 2\xi\omega)(\phi'\chi' + (\chi + \delta_1)\phi'') + (\chi + \delta_1)\xi\phi' \right) = 0, \tag{3.14}$$

with boundary conditions:

$$\begin{aligned}
f(0) = 0, f'(0) = 1 + h_1 f''(0) \left(1 + \frac{n-1}{2} We^2 \left(f''(0) \right)^2 \right), f'(\infty) = 0, \\
\theta'(0) = -\frac{Bi(1 - \theta(0))}{(1 + \varepsilon\theta(0) + \frac{4}{3}Rd)}, \theta(\infty) = 0, \\
Nb\phi'(0) + Nt\theta'(0) = 0, \phi(\infty) = 0, \\
\chi(0) = 1, \chi(\infty) = 0. \tag{3.15}
\end{aligned}$$

$\xi = \frac{1}{R} \sqrt{\frac{\nu l}{a}}$ is curvature parameter, $M^2 = \frac{\sigma \hat{B}^2 x^2}{\rho_f a l}$ is magnetic parameter, $G = \frac{\hat{E}}{B u_w^2}$ is the electric parameter, $Q = \frac{l Q^*}{\rho a C_p}$ is heat generation parameter, $K_p = \frac{\nu l}{\kappa_1 a}$ is porosity parameter, $We^2 = \frac{\Gamma^2 x^2 a^3}{\nu l^3}$ is Weissenberg number, $Rd = \frac{4\sigma^* T_\infty^3}{\kappa^* \kappa}$ is radiation parameter, $Nb = \frac{\tau D_B (C_w - C_\infty)}{C_\infty \nu}$ illustrates Brownian parameter, $Nt = \frac{\tau D_T (T_f - T_\infty)}{\nu T_\infty}$ illustrates thermophoresis constant, $E = \frac{-E_a}{\kappa_b T_\infty}$ is Arrhenius activation energy, $\gamma_r = \frac{l \kappa_r^*}{a}$

is chemical reaction parameter, $Pr = \frac{\nu}{\alpha}$ is Prandtl number, $Sc = \frac{\nu}{D_B}$ denotes the Schmidt number, $Sb = \frac{\nu}{D_m}$ illustrates the bioconvection Schmidt number, $Pe = \frac{bW_c}{D_m}$ depicts the Peclet number, $Bi = \frac{h_f}{k} \sqrt{\frac{\nu l}{a}}$ is Biot number, $h_1 = h \sqrt{\frac{a}{\nu}}$ is slip parameter, $\delta = \frac{T_f - T_\infty}{T_\infty}$ is temperature difference, $\delta_1 = \frac{N_w}{N_w - N_\infty}$ is microorganism difference parameter, $T_t = \frac{g\omega_i(T_f - T_\infty)l^2}{xu_1^2}$ is temperature buoyancy parameter, $T_c = \frac{g\omega_c(C_w - C_\infty)l^2}{xu_1^2}$ is concentration buoyancy parameter.

3.2 Physical Properties

3.2.1 Skin Friction Coefficient

C_f is a dimensionless parameter that quantifies the frictional drag experienced by a surface. It is defined as follows:

$$C_f = \frac{\dot{\tau}_w}{\frac{1}{2}\rho u_w^2}. \quad (3.16)$$

Defined the shear stress at the wall as follows:

$$\dot{\tau}_w = \dot{\mu} \left(\frac{\partial u}{\partial r} + \frac{\Gamma^2(n-1)}{2} \left(\frac{\partial u}{\partial r} \right)^3 \right)_{r=R}. \quad (3.17)$$

Using equation (3.17) in equation (3.16) we get:

$$\frac{C_f Re_x^{-\frac{1}{2}}}{2} = f''(0) + \frac{(n-1)}{2} We^2 \left(f''(0) \right)^3. \quad (3.18)$$

Here, the local Reynolds number is given as: $Re_x = \frac{u_w x}{\nu}$.

3.2.2 Local Nusselt Number

To analyze the heat transfer rate at the wall, we illustrate the value of Nu_x at the surface.

$$Nu_x = \frac{x \hat{q}_w}{\kappa(T_f - T_\infty)}. \quad (3.19)$$

where heat flux is defined as:

$$q_w = -\kappa \left(\frac{\partial T}{\partial r} \right)_{r=R} + q_r. \quad (3.20)$$

Using equation (3.20) in equation (3.19) we get:

$$Nu_x Re_x^{-\frac{1}{2}} = - \left(1 + \frac{4Rd}{3(1 + \epsilon\theta(0))} \right) \theta'(0). \quad (3.21)$$

3.2.3 Local Sherwood Number

The Sh_x is defined as:

$$Sh_x = \frac{xj^*_{*w}}{D_B(C_W - C_\infty)}. \quad (3.22)$$

Fick's law can be used to express the mass transfer as:

$$j^*_{*w} = -D_B \left(\frac{\partial C}{\partial r} \right)_{r=R}. \quad (3.23)$$

Using equation (3.23) in equation (3.22) we get:

$$Sh_x Re_x^{-\frac{1}{2}} = -\phi'(0). \quad (3.24)$$

3.2.4 Local Density Of Motile Microorganisms

The Nn_x is determined by:

$$Nn_x = \frac{xi^*_{*w}}{D_m(N_W - N_\infty)}. \quad (3.25)$$

Where:

$$i^*_{*w} = -D_m \left(\frac{\partial N}{\partial r} \right)_{r=R}. \quad (3.26)$$

Using equation (3.26) in equation (3.24) we get:

$$Nn_x Re_x^{-\frac{1}{2}} = -\chi'(0). \quad (3.27)$$

3.3 Numerical Approach

In order to solve the group of differential equations (3.11)–(3.14) and their corresponding boundary conditions (3.15), we employed a numerical method called *bvp4c*. We solved the first-order differential equations and established an initial value problem. To facilitate this, we introduced converted variables, which allowed us to create the necessary set of first-order differential equations. With the aid of these transformed variables, we successfully solved the first-order differential equations.

$$\begin{aligned}
 f &= \Upsilon_1, \quad f' = \Upsilon'_1 = \Upsilon_2, \quad f'' = \Upsilon'_2 = \Upsilon_3, \\
 \theta &= \Upsilon_4, \quad \theta' = \Upsilon'_4 = \Upsilon_5, \\
 \phi &= \Upsilon_6, \quad \phi' = \Upsilon_7, \\
 \chi &= \Upsilon_8, \quad \chi' = \Upsilon'_8 = \Upsilon_9,
 \end{aligned} \tag{3.28}$$

$$\begin{aligned}
 \Upsilon'_3 &= \left(\frac{1}{(1 + 2\xi\omega) + \frac{3(n-1)}{2}(1 + 2\xi\omega)^2 We^2(\Upsilon_3)^2} \right) \left(-2\xi\Upsilon_3 - \frac{(n-1)}{2} We^2\xi(1 + 2\xi\omega)(\Upsilon_3)^3 \right. \\
 &\quad \left. - \frac{3(n-1)}{2} We^2\xi(1 + 2\xi\omega)(\Upsilon_3)^3 + M^2(\Upsilon_2 - G) + Kp\Upsilon_2 \right. \\
 &\quad \left. + (\Upsilon_2)^2 - (T_t + T_c)\cos(\gamma) - \Upsilon_1\Upsilon_3 \right),
 \end{aligned} \tag{3.29}$$

$$\begin{aligned}
 \Upsilon'_5 &= \left(\frac{1}{(1 + 2\xi\omega)(1 + \varepsilon\Upsilon_4) + \frac{4}{3}(1 + 2\xi\omega)Rd} \right) \left(-2\xi(1 + \varepsilon\Upsilon_4)\Upsilon_5 - (1 + 2\xi\omega)\varepsilon(\Upsilon_5)^2 - \right. \\
 &\quad \left. Pr(1 + 2\xi\omega)(Nt(\Upsilon_5)^2 + Nb\Upsilon_5\Upsilon_7) - Pr(Q\Upsilon_4 + \Upsilon_1\Upsilon_5) - \frac{4}{3}2\xi Rd\Upsilon_5 \right),
 \end{aligned} \tag{3.30}$$

$$\begin{aligned}
 \Upsilon'_7 &= \left(\frac{1}{(1 + 2\xi\omega)} \right) \left(-2\xi\Upsilon_7 - 2\xi\frac{Nt}{Nb}\Upsilon_5 - (1 + 2\xi\omega)\frac{Nt}{Nb}\Upsilon'_5 - Sc\Upsilon_1\Upsilon_7 + \right. \\
 &\quad \left. \gamma_r Sc(1 + \delta\Upsilon_4)^m \Upsilon_6 \exp\left(\frac{-E}{1 + \delta\Upsilon_4}\right) \right),
 \end{aligned} \tag{3.31}$$

$$\begin{aligned}
 \Upsilon'_9 &= \left(\frac{1}{(1 + 2\xi\omega)} \right) \left(-2\xi\Upsilon_9 - Sb\Upsilon_1\Upsilon_9 + Pe((1 + 2\xi\omega)(\Upsilon_7\Upsilon_9 + (\delta_1 + \Upsilon_8)\Upsilon'_7) + (\delta_1 + \Upsilon_8)\xi\Upsilon_7) \right),
 \end{aligned} \tag{3.32}$$

$$\Upsilon_1(0) = 0, \quad \Upsilon_2(0) = 1 + h_1 \Upsilon_3(0) \left(1 + \frac{n-1}{2} We^2 (\Upsilon_3(0))^2 \right), \quad \Upsilon_2(\infty) = 0, \quad (3.33)$$

$$\Upsilon_5(0) = -\frac{Bi(1 - \Upsilon_4(0))}{1 + \varepsilon \Upsilon_4(0) + \frac{4}{3} Rd}, \quad \Upsilon_4(\infty) = 0, \quad (3.34)$$

$$Nb\Upsilon_7(0) + Nt\Upsilon_5(0) = 0, \quad \Upsilon_6(\infty) = 0, \quad (3.35)$$

$$\Upsilon_8(0) = 1, \quad \Upsilon_8(\infty) = 0. \quad (3.36)$$

3.4 Result and Discussion

3.4.1 Discussion of Tables

The current numerical findings of $\frac{C_f(Re)^{-\frac{1}{2}}}{2}$ for various values of ξ are compared to the corresponding published results in Table 3.1. Based on the statistics, the current numerical findings demonstrate a high level of accuracy in comparison to the published data. Table 3.2 represents the dynamic of numerous variables on C_f . Increment in the values of ξ , M and Kp parameters the C_f increases, and negligible effect on C_f when we increment in the values n , G , T_i , T_c and γ . It dwindles when we increase the value of We and h_1 . Table 3.3 represents the dynamic of numerous variables on Nu_x . When Pr , and Bi are increased, Nu_x also increases. There is no effect on Nu_x when we increase the values of the ξ , Nt , ε , and Nb . However, it dwindles when boosted the values of Q , and Rd . Table 3.4 represents the dynamic of numerous parameters on Sh_x . When increased the values of Nt parameters the Sh_x increases. It is no effect on Nu_x when we increased the values ξ , E , m , γ_r , Sc , and δ and it dwindles when we increased the values of Nb . Table 3.5 represents the dynamic of numerous parameters on Nn_x . As we increased the values of ξ , and Sb the Nn_x also increases. It dwindles when we increased the values of Pe , and δ_1 .

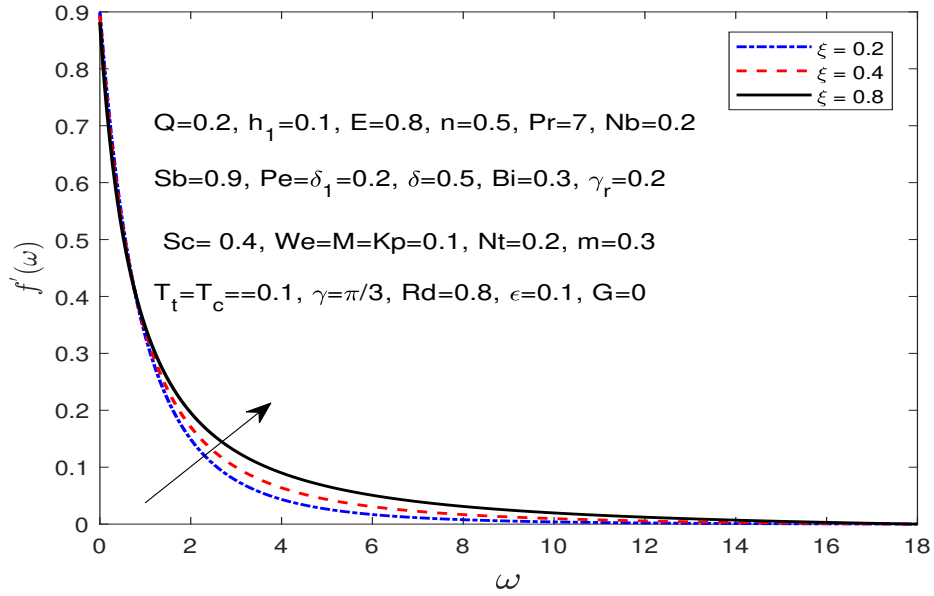


Figure 3.2: The velocity dependence on ξ .

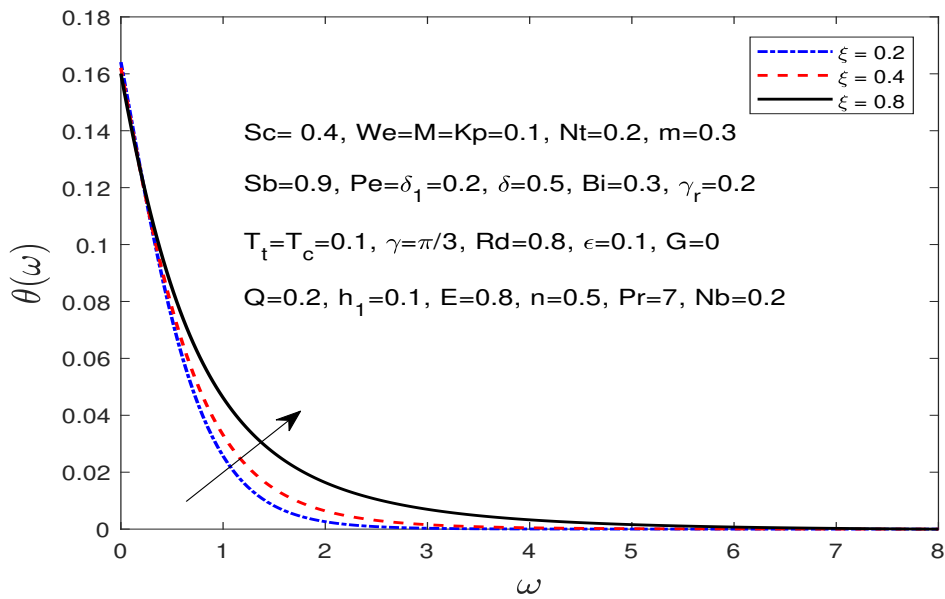


Figure 3.3: The temperature dependence on ξ .

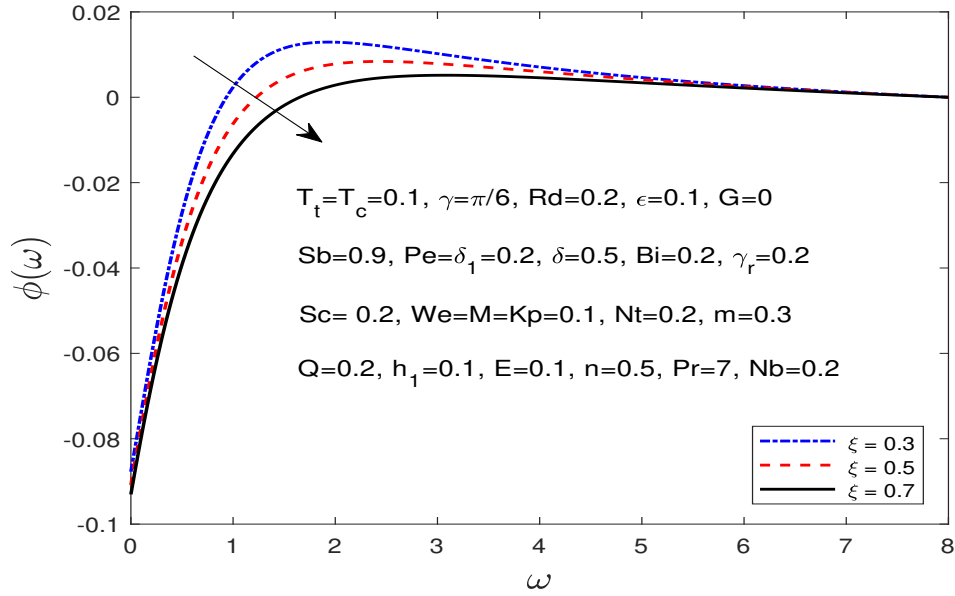


Figure 3.4: The concentration dependence on ξ .

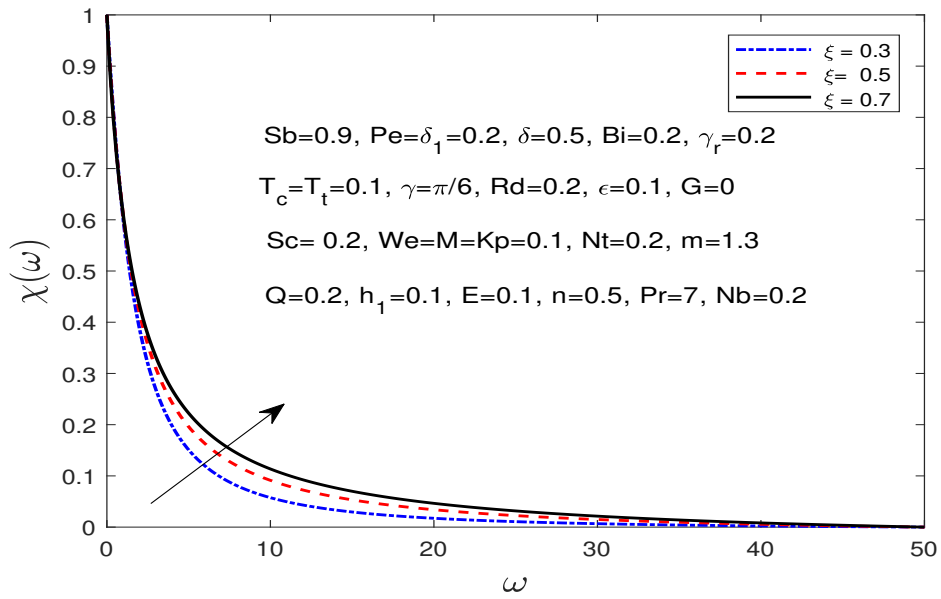


Figure 3.5: The motile microorganisms dependence on ξ .

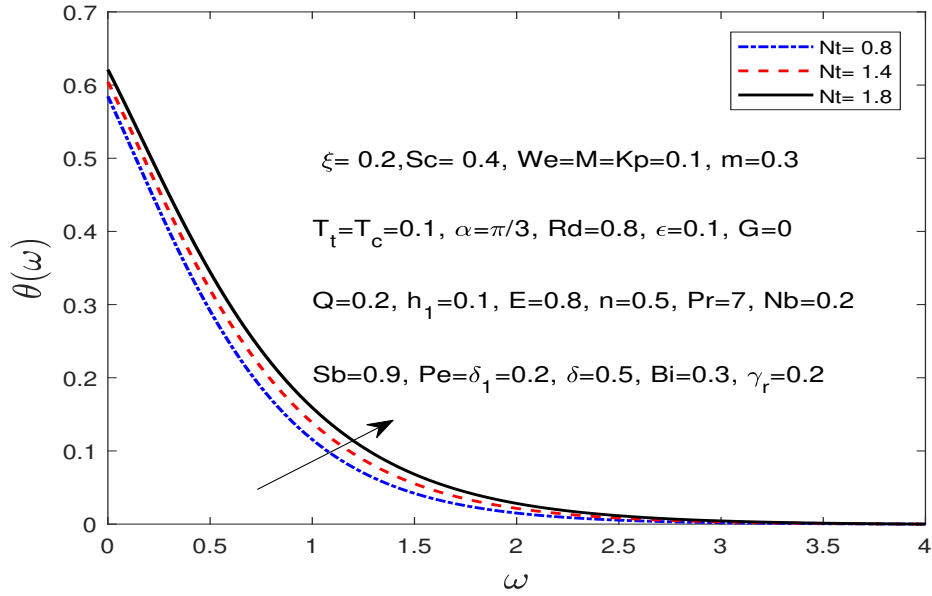


Figure 3.6: The temperature dependence on Nt .

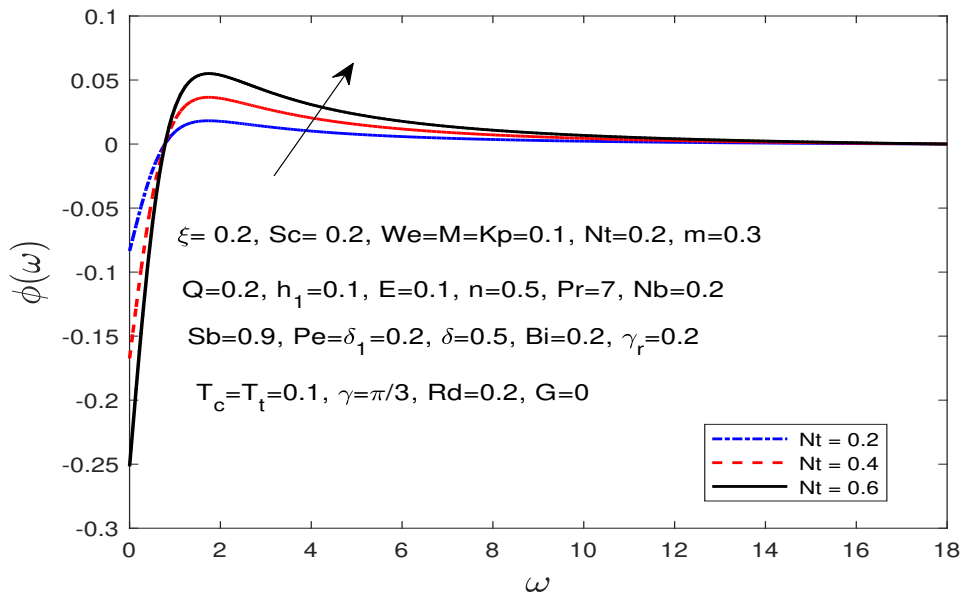


Figure 3.7: The concentration dependence on Nt .

ξ	Rangi and Ahmad [28]	Hashim et al. [29]	Current result
0	-1.0000	-1.0000	-1.0000
0.25	-1.094378	-1.094373	-1.090626
0.5	-1.188715	-1.188727	-1.178434
0.75	-1.281833	-1.281819	-1.263496

Table 3.1: During the examination of how $\frac{C_f(Re_x)^{-\frac{1}{2}}}{2}$ changes with different values of ξ , we take into account the following parameter values: $We = G = M = Kp = h_1 = T_t = T_C = 0$ and $n = 1$.

3.4.2 Discussion of Graphs

Fig.3.2 represents the effect of ξ on velocity rate. The correlation between ξ and radius is inverse. The cylinder radius dwindles when ξ increases, thereby reducing the resistance of the fluid that increased the velocity profile. Fig.3.3 demonstrates that the temperature profile is boosted when ξ increases because the velocity rate is enhanced, which increases the mobility of fluid particles, which, in turn, leads to an increased trend in temperature distribution. Fig.3.4 represents decreasing trend in concentration rate when increments in the ξ . The reason behind this phenomenon is the observed velocity and temperature distribution increasing, leading to variations in the fluid's viscosity. As the fluid's viscosity decreases, it enhances the motion of nanoparticles, ultimately causing a decrease in concentration. Fig.3.5 represents an increasing trend in microorganisms profile when increment in xi . The reason behind this phenomenon is the motion of nanoparticles increased that increasing speed of cells and getting interact with each other.

Fig.3.6 demonstrates that as we increase the Nt , the temperature profile also increases. Near the boundary line, the concentration distribution dwindles because, near the boundary line, the temperature difference is greater, which causes the transportation of nanoparticles to be higher. As we move away from the boundary line, the

ξ	We	M	Kp	h_1	T_t	T_c	n	G	$-\frac{C_f(Re)^{-\frac{1}{2}}}{2}$
0.3	0.1	0.1	0.2	0.1	0.1	0.1	0.5	0	1.04347
0.5	-	-	-	-	-	-	-	-	1.10082
0.5	-	-	-	-	-	-	-	-	1.15564
0.3	0.1	-	-	-	-	-	-	-	1.04347
-	0.3	-	-	-	-	-	-	-	1.03766
-	0.5	-	-	-	-	-	-	-	1.02491
-	0.1	0.1	-	-	-	-	-	-	1.04347
-	-	0.5	-	-	-	-	-	-	1.13116
-	-	0.7	-	-	-	-	-	-	1.20907
-	-	0.1	0.2	-	-	-	-	-	1.04347
-	-	-	0.4	-	-	-	-	-	1.11731
-	-	-	0.6	-	-	-	-	-	1.18401
-	-	-	0.2	0.1	-	-	-	-	1.04347
-	-	-	-	0.3	-	-	-	-	0.823973
-	-	-	-	0.5	-	-	-	-	0.685804
-	-	-	-	0.1	0.1	-	-	-	1.04347
-	-	-	-	-	0.5	-	-	-	1.02929
-	-	-	-	-	0.7	-	-	-	1.02229
-	-	-	-	-	0.1	0.1	-	-	1.04347
-	-	-	-	-	-	0.5	-	-	1.04763
	-	-	-	-	-	0.7	-	-	1.04972
	-	-	-	-	-	0.1	0.4	-	1.04333
	-	-	-	-	-	-	0.6	-	1.04361
	-	-	-	-	-	-	0.8	-	1.04389
	-	-	-	-	-	-	0.5	0	1.04347
	-	-	-	-	-	-	-	0.1	1.04194
	-	-	-	-	-	-	-	0.3	1.03890

Table 3.2: Considering the consequences of numerous factors regarding the coefficient of skin friction $\varepsilon = 0.1, Nt = 0.1, Q = 0.1, Rd = 0.8, Sc = E = 0.2, \delta = 0.2, \gamma_r = 0.8, \gamma = \pi/4, m = 1.3, Nb = 0.1, Sb = 0.5, Pe = \delta_1 = 0.2, Bi = 0.3, Pr = 7.$

transportation of nanoparticles decreases, which causes the concentration distribution to increase, as demonstrated by the impact of Nt in Fig.3.7. Fig.3.8 represents that surging the value of Kp results in declines in velocity rate this is due to the fact that higher permeability implies a greater hindrance to the fluid's movement, leading to

ξ	Nt	ε	Pr	Nb	Rd	Bi	Q	$-\theta'(0)$
0.2	0.2	0.3	7	0.4	0.3	0.5	0.1	0.357299
0.5	-	-	-	-	-	-	-	0.361166
0.7	-	-	-	-	-	-	-	0.363476
0.2	0.2	-	-	-	-	-	-	0.357299
-	0.5	-	-	-	-	-	-	0.356974
-	0.7	-	-	-	-	-	-	0.356754
-	0.2	0.3	-	-	-	-	-	0.357299
-	-	0.5	-	-	-	-	-	0.334754
-	-	0.7	-	-	-	-	-	0.314067
-	-	0.3	5.1	-	-	-	-	0.341082
-	-	-	6	-	-	-	-	0.349699
-	-	-	7	-	-	-	-	0.357299
-	-	-	7	0.4	-	-	-	0.357299
-	-	-	-	0.7	-	-	-	0.357298
-	-	-	-	0.9	-	-	-	0.357299
-	-	-	-	0.4	0.3	-	-	0.357299
-	-	-	-	-	0.5	-	-	0.371649
-	-	-	-	-	0.7	-	-	0.381959
-	-	-	-	-	0.3	0.5	-	0.357299
-	-	-	-	-	-	0.7	-	0.448751
-	-	-	-	-	-	0.9	-	0.523051
-	-	-	-	-	-	0.5	0.1	0.357299
-	-	-	-	-	-	-	0.3	0.318111
-	-	-	-	-	-	-	0.7	0.337158

Table 3.3: Evaluating the consequences of numerous factors affecting the Nusselt index $We = M0.2$, $Kp = 0.1$, $n = 0.5$, $G = 0.1$, $h_1 = 0.1$, $T_t = T_c = 0.1$, $\gamma = \pi/3$, $E = 0.2$, $Sc = 0.1$, $\delta = \gamma_r = 0.8$, $Sb = \delta_1 = Pe = 0.2$, $m = 1.3$.

a reduction in its speed. Therefore, when the permeability parameter is raised, the velocity of the fluid decreases. When the magnetic field strength is heightened, the velocity profile experiences a decline as a result of the creation of a Lorentz force. This force acts in a way that hinders the fluid's mobility, resulting in declines in velocity rate. Consequently, by increasing the M , the velocity is effectively reduced which represents Fig.3.9. Fig.3.10 represents the dynamics of T_t on the velocity rate. As we increased the value of T_t , the velocity rate increased due to an increment in T_i , which

ξ	E	Nt	m	Nb	γ_r	Sc	δ	$-\phi'(0)$
0.2	1.1	0.2	1.3	0.4	0.8	0.1	0.2	0.135505
0.6	-	-	-	-	-	-	-	0.137542
0.9	-	-	-	-	-	-	-	0.138873
0.2	1.1	-	-	-	-	-	-	0.135505
-	1.3	-	-	-	-	-	-	0.135508
-	1.5	-	-	-	-	-	-	0.135511
-	1.1	0.2	-	-	-	-	-	0.135505
-	-	0.4	-	-	-	-	-	0.270902
-	-	0.9	-	-	-	-	-	0.608914
-	-	0.2	1.3	-	-	-	-	0.135505
-	-	-	1.5	-	-	-	-	0.135505
-	-	-	1.7	-	-	-	-	0.135505
-	-	-	1.3	0.4	-	-	-	0.135505
-	-	-	-	0.6	-	-	-	0.090337
-	-	-	-	0.8	-	-	-	0.067753
-	-	-	-	0.4	0.8	-	-	0.135505
-	-	-	-	-	1.2	-	-	0.135495
-	-	-	-	-	1.7	-	-	0.135483
-	-	-	-	-	0.8	0.1	-	0.135505
-	-	-	-	-	-	0.3	-	0.135421
-	-	-	-	-	-	0.5	-	0.135348
-	-	-	-	-	-	0.1	0.2	0.135505
-	-	-	-	-	-	-	0.5	0.135503
-	-	-	-	-	-	-	0.8	0.135501

Table 3.4: Evaluating the consequences of numerous factors affecting the Sherwood index $We = M = 0.2$, $Kp = 0.1$, $n = 0.5$, $G = 0$, $h_1 = 0.1$, $T_t = T_c = 0.1$, $\gamma = \frac{\pi}{3}$, $\varepsilon = 0.3$, $Bi = 0.5$, $Pr = 7$, $Q = 0.1$, $\delta_1 = 0.8$, $Sb = Pe = 0.2$, $Rd = 0.3$.

led to an increase in buoyancy forces that caused the fluid to become lighter. Fig.3.11 represents the dynamics of T_c on the velocity distribution. As we increased the value of T_c , the velocity rate decreased due to fluids having high movement of nanoparticles, which resulted in a decrease in the movement of fluid.

Fig.12 represents the dynamics of Bi on the transfer rate of heat. An enhancement in Bi indicates a more efficient advection at the solid-liquid interface, resulting in a rapid

Sb	ξ	Pe	δ_1	$-\chi'(0)$
0.9	0.2	0.3	0.3	0.525645
1.3	-	-	-	0.671561
1.6	-	-	-	0.768024
0.9	0.2	-	-	0.525645
-	0.4	-	-	0.574553
-	0.6	-	-	0.630781
-	0.2	0.3	-	0.525645
-	-	0.5	-	0.501422
-	-	0.7	-	0.480562
-	-	0.3	0.3	0.525645
-	-	-	0.7	0.512810
-	-	-	1.2	0.500947

Table 3.5: Impact of various factors on the motile microorganisms by taking into consideration $We = Kp = We = 0.1$, $n = 0.5$, $G = 0$, $h_1 = 0.1$, $T_i = W_r = S_b = 0.1$, $J = \pi/3$, $\varepsilon = 0.3$, $Nt = 0.2$, $Q = 0.1$, $Rd = 0.3$, $Sc = 0.1$, $E = 0.2$, $\delta = 0.2$, $\gamma_r = 0.8$, $m = 1.3$, $Nb = 0.4$, $Bi = 0.3$, $Pr = 7$.

exchange of thermal energy between the solid and fluid. Consequently, the temperature distribution increases. Fig.3.13 represents the influence of Rd on temperature profile. When increased the radiation of the system, the fluid particles absorb more heat, leading to an increasing trend in the temperature profile. The heat transfer rate has an inverse relationship with Pr because an increment in Pr caused an increase in the heat conduction of the system, resulting in a decline in the convective heat transfer rate. This decline caused a temperature distribution decrease, as demonstrated in Fig.3.14. Fig.3.15 represents the influence of γ_r on the slope of concentration. An increment in the γ_r reduces the motion of fluid concentration, resulting in less chemical diffusion. Fig.3.16 represents the influence of Sc on the slope of concentration. Increments in Sc causes the concentration rate to decrease. An increment in the value of Nb caused a reduction in concentration rate as represented in Fig.3.17. Fig.3.18 represents the influence of the effect of Sb . An increment in Sb causes a reduction in the diffusion of microorganisms, leading to a decline in the density of microorganisms and the thick-

ness of the boundary layer. In Fig.3.19, Fig.3.20 and Fig.3.21, the slope of the curves decreases as we increment the values of We , h_1 , and T_t , respectively, and plot them against M . Similarly, in Fig.3.22 the slope of the curves decreases as we increment in the values of Bi that plot against ε . In Fig.3.23 the C_f is increased when increment in the values of Pr .

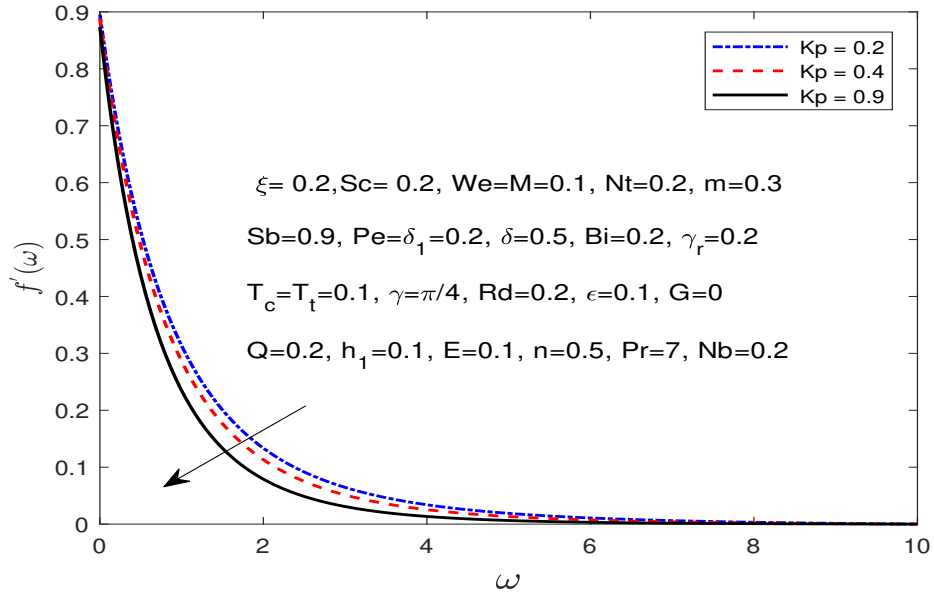


Figure 3.8: The velocity dependence on Kp .

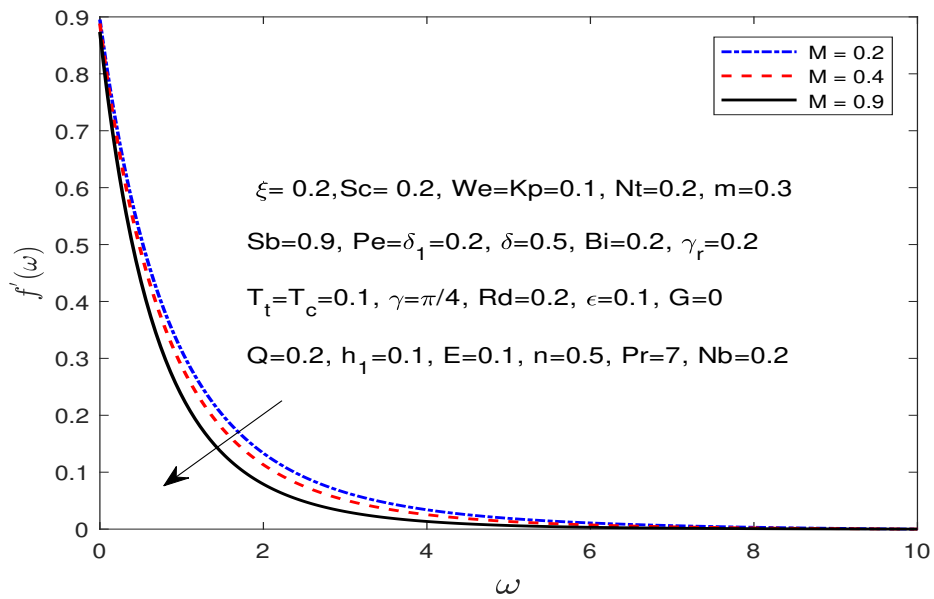


Figure 3.9: The velocity dependence on M .

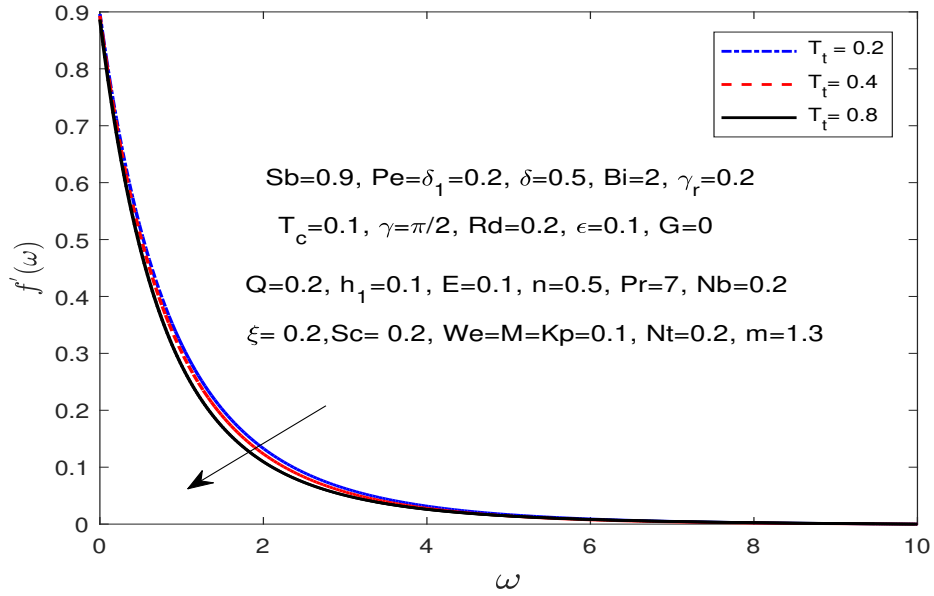


Figure 3.10: The velocity dependence on T_t .

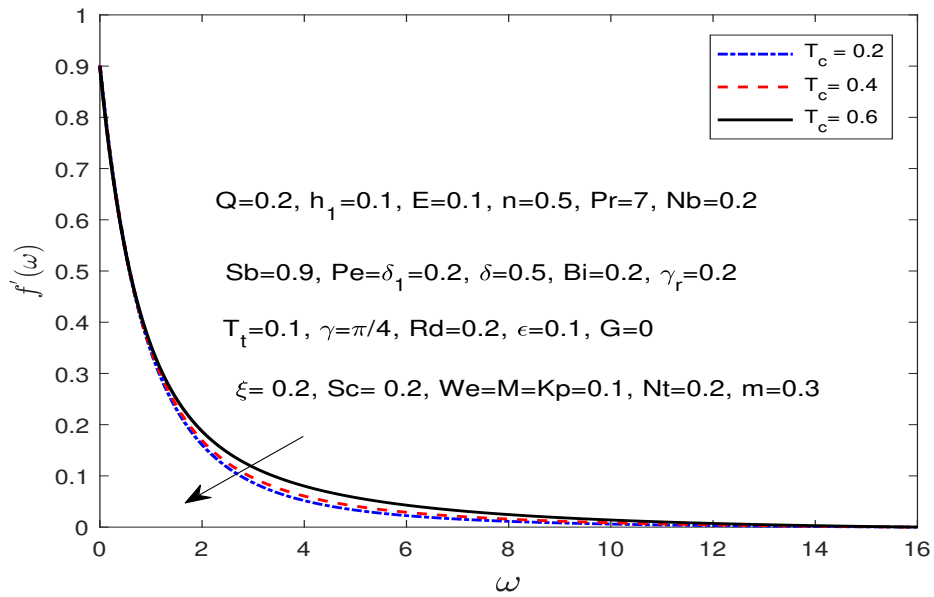


Figure 3.11: The velocity dependence on T_c .

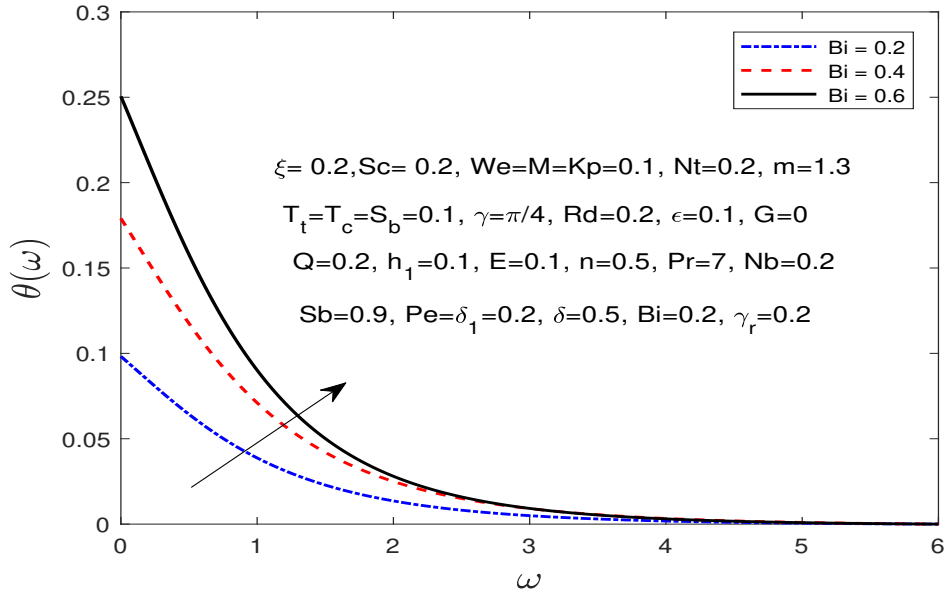


Figure 3.12: The temperature dependence on Bi .

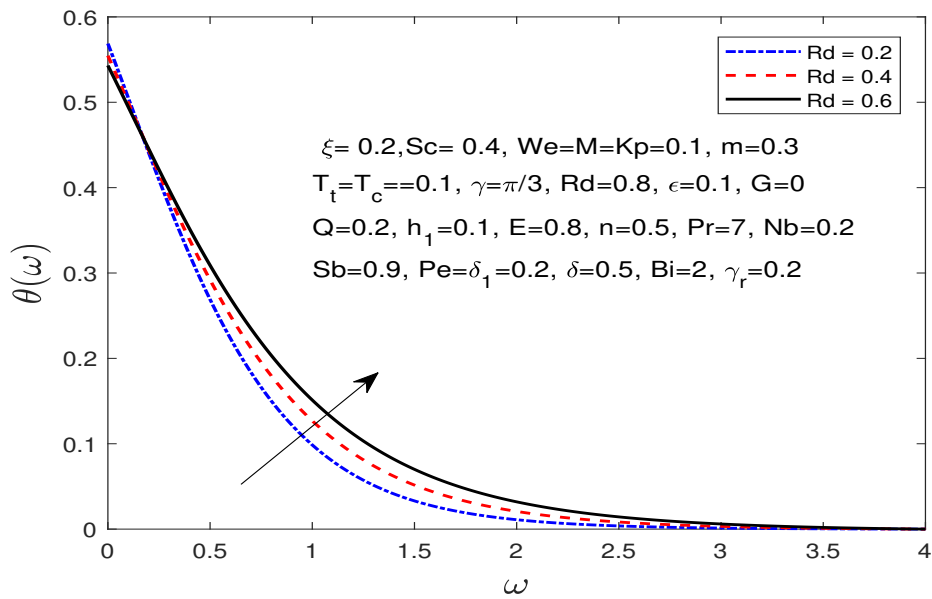


Figure 3.13: The temperature dependence on Rd .

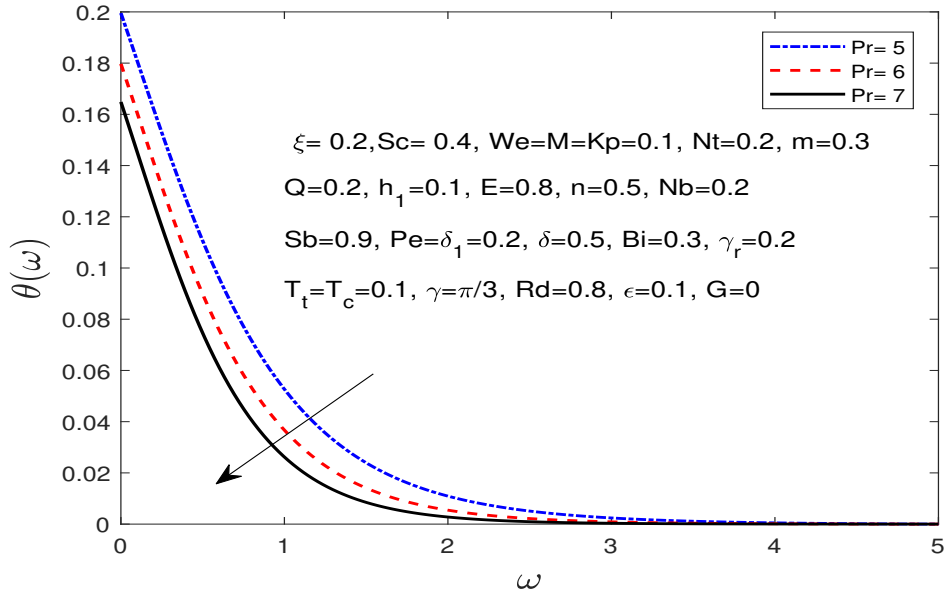


Figure 3.14: The temperature dependence on Pr .

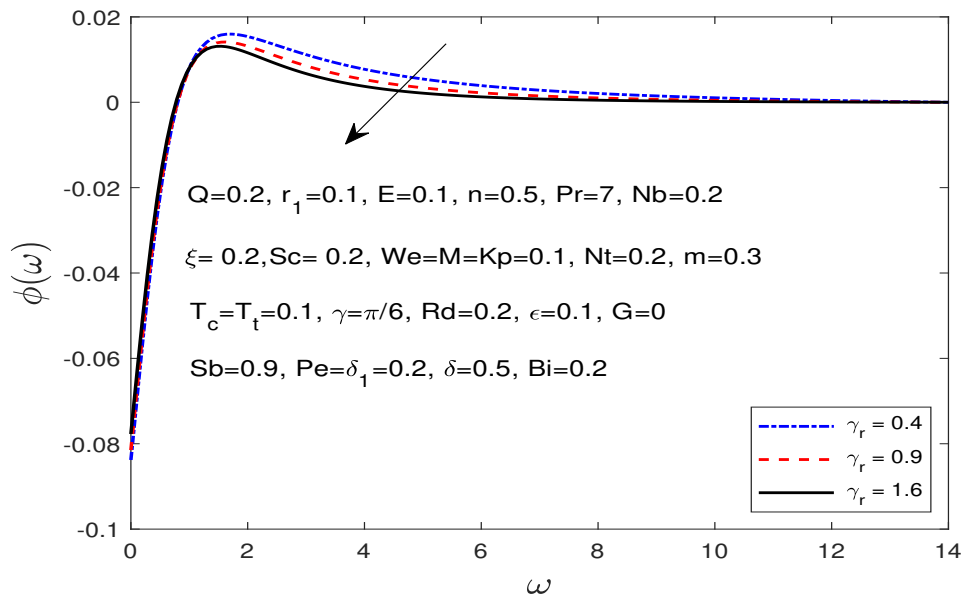


Figure 3.15: The concentration dependence on γ_r .

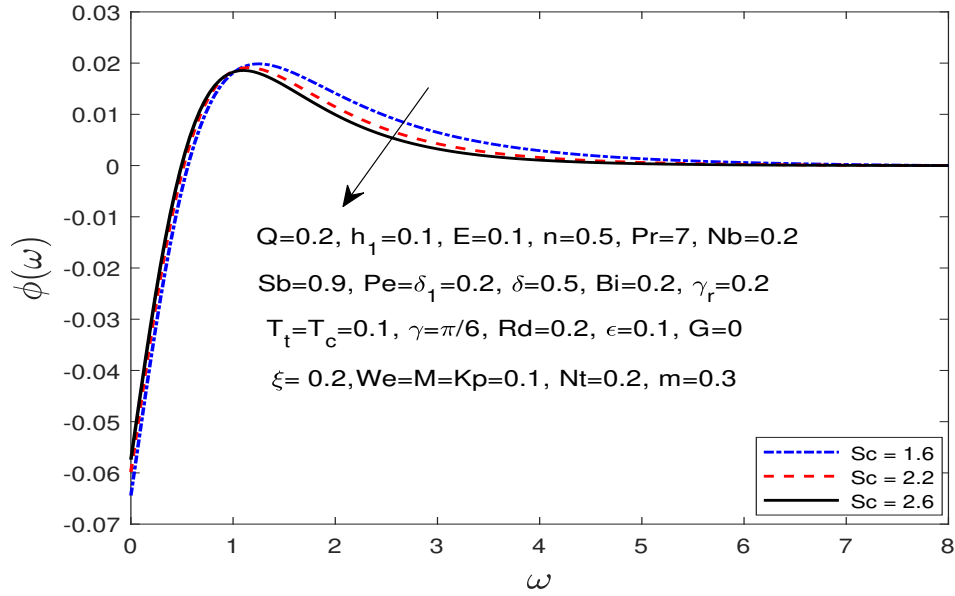


Figure 3.16: The concentration dependence on Sc .

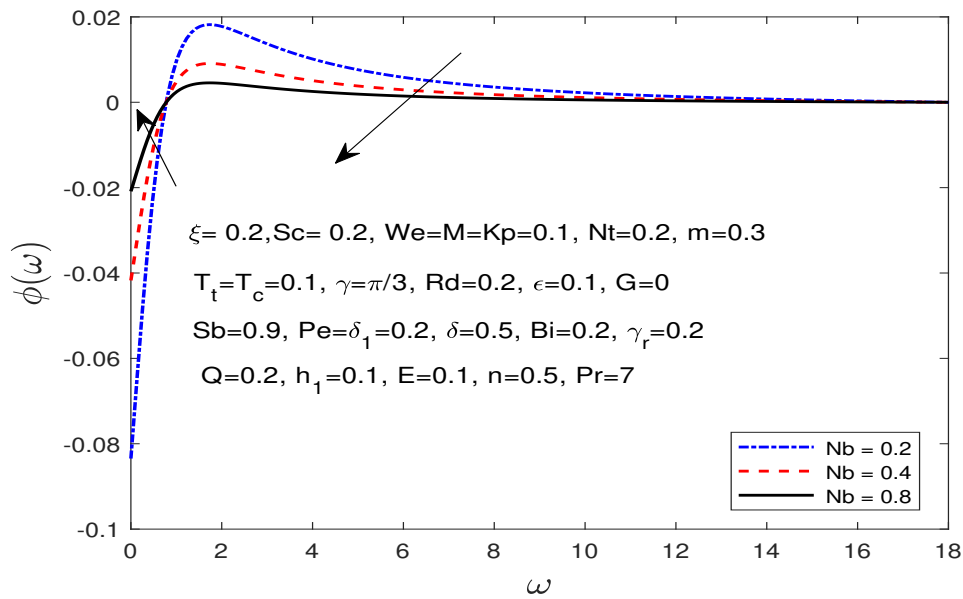


Figure 3.17: The concentration dependence on Nb .

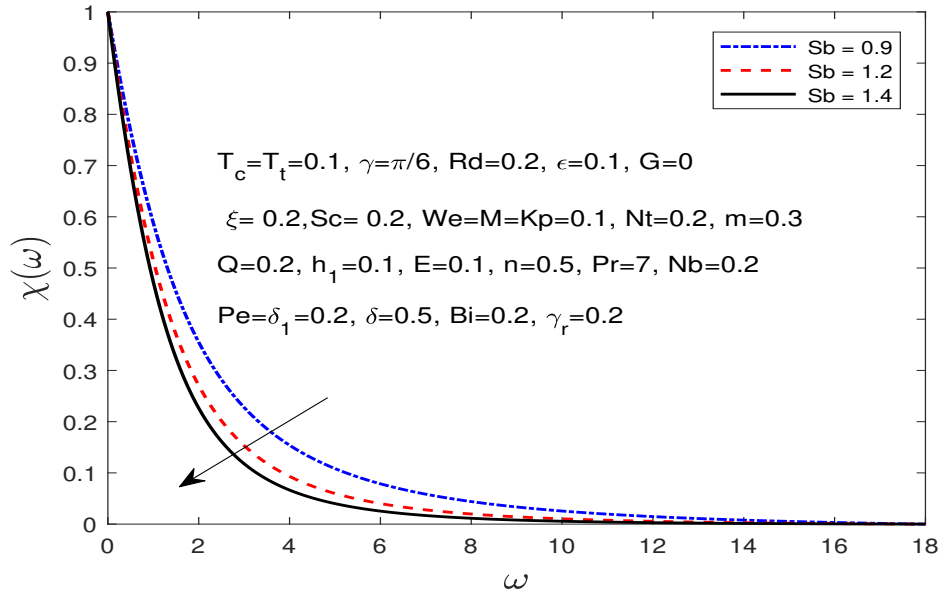


Figure 3.18: The motile microorganism dependence on Sb .

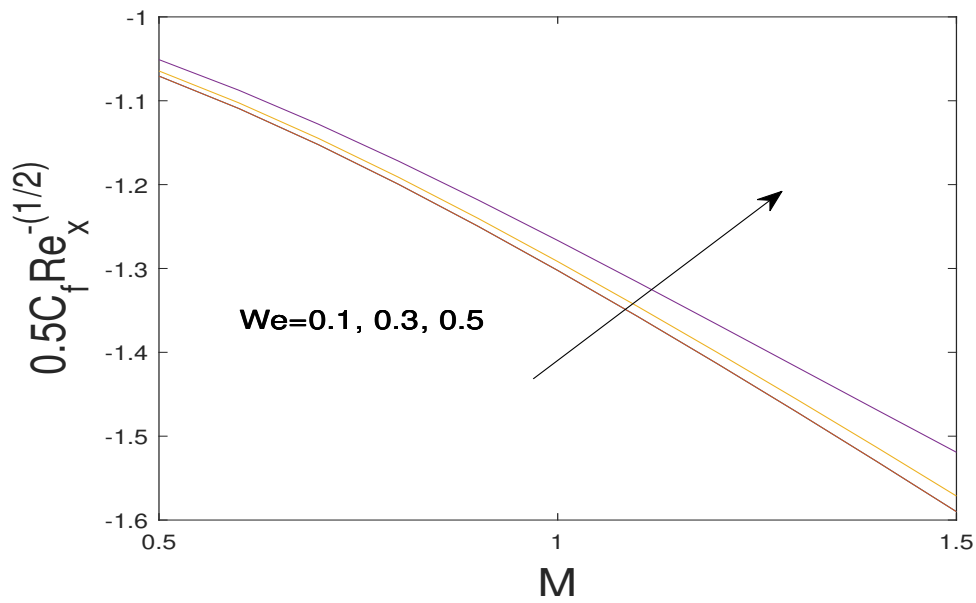


Figure 3.19: Effect of We on skin friction coefficient.

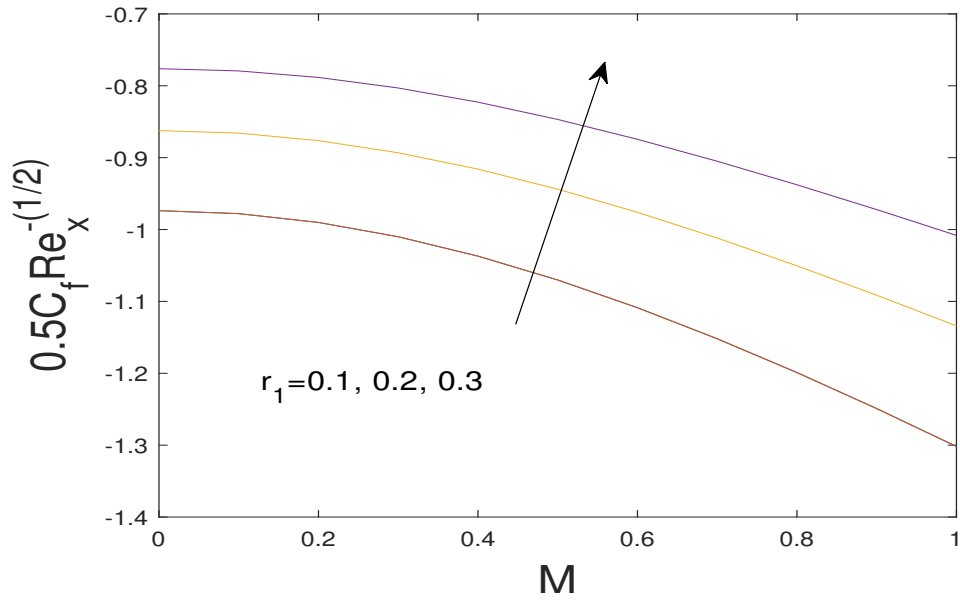


Figure 3.20: Effect of h_1 on on skin friction coefficient.

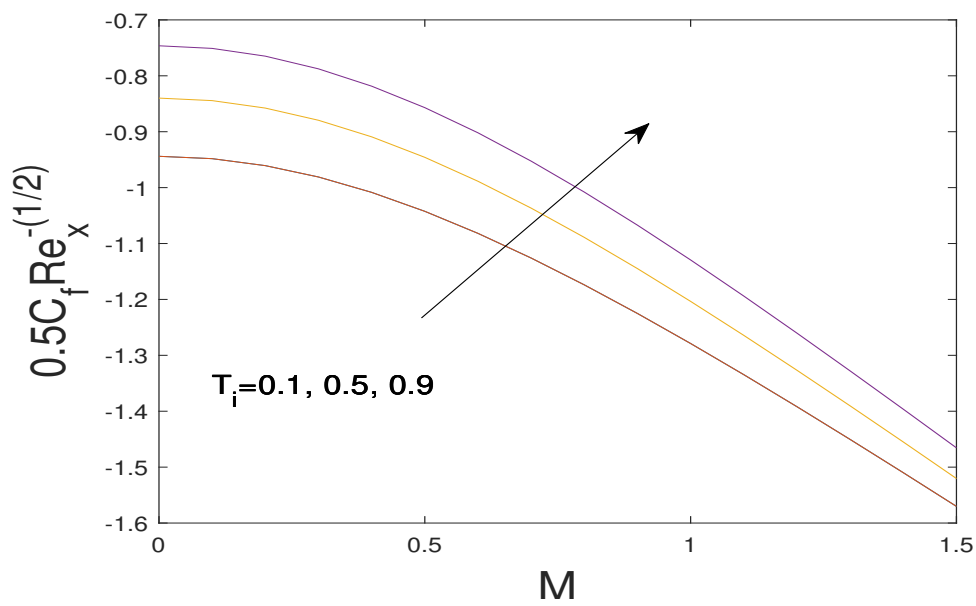


Figure 3.21: Effect of T_i on skin friction coefficient.

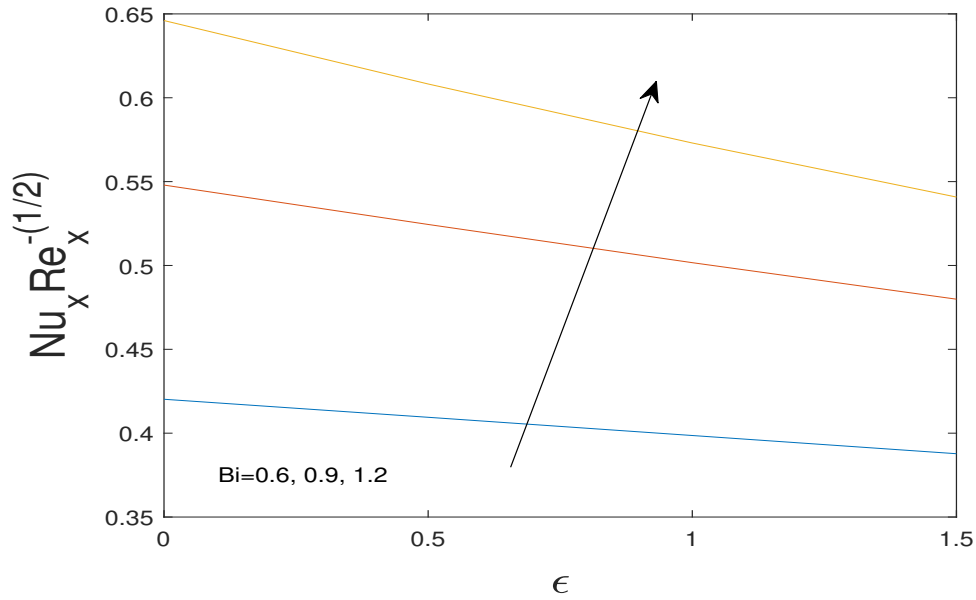


Figure 3.22: Effect of Bi on local Nusselt number.

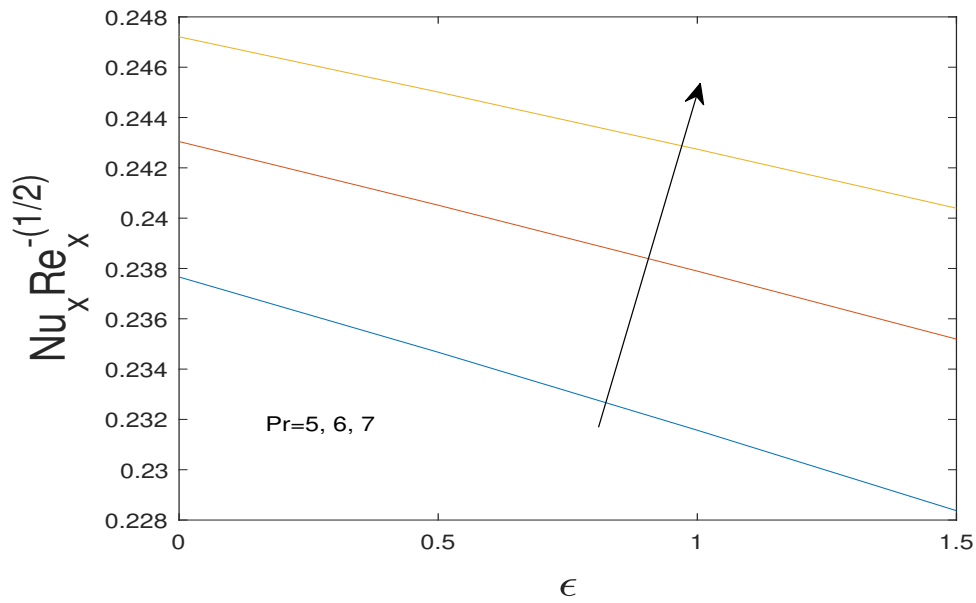


Figure 3.23: Effect of Pr on local Nusselt number.

Chapter 4

Conclusion

The thesis is primarily divided in three chapters. In the first chapter, a brief note is given along with basic definitions of fluid and its classes like Newtonian and non-Newtonian fluids. The various properties of fluid flow like compressible, incompressible, steady, unsteady, and MHD flow is also explained. The conservation laws of mass, momentum, and energy are also described. Dimensionless parameters like Reynolds number, Prandtl number, and Biot number are briefly mentioned. Lastly, the numerical methods are discussed.

In chapter two, we explored the extended problem of the impact of implications of convection, with an emphasis on thermal radiation and chemical reaction for a flow of a Carreau nanofluid over a stretching cylinder considering a permeable medium. The governing equations were transformed into ODEs using similarity variables. Following the transformation the **bvp4c** was applied using MATLAB. The results attained for the influence of various parameters on the dimensionless parameters like density of motile microorganisms etc. are tabulated. Graphical representation is also provided for impact of parameters on velocity, temperature, solute distribution, and motile microorganisms. A few of the notable findings are:

- Velocity profile decreases as the Kp , and M values increases and increases as the

α^* value increases.

- The temperature profile boosted as the α^* , Bi , and Rd value increases and dwindles as the Pr , and Nb values raised.
- The concentration profile decreases as the α_* , γ_r , Sc , and Nb value increases, and increases as the Nt , E parameters values increase.
- The motile microorganisms profile increases as α_* , and the Nt value increases, and decreases as the Sb parameter values increase.
- Boosting the values of α^* , M , and Kp simultaneously enhances C_f .
- The α_* , Bi , and Pr simultaneously enhance the Nu_x . When the values of Rd and Q are increased, the value of the Nu_x decreases.
- An increment in Nb , and α^* values, the local Sherwood number falls, but it increases when the Nt value rises.
- As Sb , and α_* increase, the concentration of motile microorganisms shows an upward trend, but when the Pe value rises, it falls.

In chapter three, we explored the extended problem of the impact of variable EMHD Carreau Nanofluid slip flow over an inclined cylinder with chemical reaction and variable thermal conductivity in the presence of a porous medium. PDEs are transformed into a set of coupled ODEs when non-similarity variables are introduced. An extensively employed collocation-based MATLAB tool called *bvp4c* is implemented to compute the results. Graphs represent the dynamics of numerous parameters on the concentration, temperature, velocity, and microorganism profiles. Tables represent the impact of numerous parameters on the physical properties of local Nusselt number, skin

friction coefficient, rate of transfer of microorganisms at cylinder, and local Sherwood number. A few of the notable findings are:

- Velocity profile diminishes when boosted the Kp and M values, whereas it increased with rise in the ξ values.
- Temperature distribution surged when raised in the ξ , and Rd values and declines as the values of Pr surged.
- As the ξ , γ_r , and Nb values surged, the concentration distribution declined and incremented as do the Nt parameter values.
- As the Kp , M , and ξ values surged caused increments in C_f .
- An increase in the values of Pr , and Bi caused increments in Nu_x .
- Higher values of Nb lead to a declines in the value of Sh_x . Boosted the values of Sb , and ξ caused increments in Nn_x .

Bibliography

- [1] P. J. Carreau, Rheological equations from molecular network theories, *Transactions of the Society of Rheology* 16 (1) (1972) 99-127.
- [2] R. B. Bird, C. F. Curtiss, R. C. Armstrong, and O. Hassager, *Dynamics of polymeric liquids, Kinetic theory*. Wiley 2 (1987).
- [3] H. A. Barnes, J. F. Hutton, and K. Walters, *An introduction to rheology*, Elsevier 3 (1989).
- [4] K. Khellaf, and G. Lauriat, Numerical study of heat transfer in a non-Newtonian Carreau-fluid between rotating concentric vertical cylinders, *Journal of non-Newtonian Fluid Mechanics* 89 (1-2) (2000) 45-61.
- [5] N. S. Akbar, S. Nadeem, R. U. Haq, and Y. Shiwei, MHD stagnation point flow of Carreau fluid toward a permeable shrinking sheet: Dual solutions, *Ain Shams Engineering Journal* 5 (4) (2014) 1233-1239.
- [6] M. Khan, and H. Hashim, Boundary layer flow and heat transfer to Carreau fluid over a nonlinear stretching sheet, *AIP Advances* 5 (10) (2015).
- [7] M. Waqas, M. Farooq, M. I. Khan, A. Alsaedi, T. Hayat, and T. Yasmeen, Magnetohydrodynamic (MHD) mixed convection flow of micropolar liquid due to nonlinear stretched sheet with convective condition, *International Journal of Heat and Mass Transfer* 102 (2016) 766-772.

- [8] M. Waqas, T. Hayat, M. Farooq, S. A. Shehzad, and A. Alsaedi, Cattaneo-Christov heat flux model for flow of variable thermal conductivity generalized Burgers fluid, *Journal of Molecular Liquids* 220 (2016) 642-648.
- [9] S. U. S. Choi, and J. A. Eastman, Enhancing thermal conductivity of fluids with nanoparticles. No. ANL/MSD/CP-84938; CONF-951135-29, Argonne National Lab.(ANL), Argonne, IL (United States) (1995).
- [10] J. Buongiorno, Convective transport in nanofluids, *J. Heat Transfer* 128 (3) (2006) 240-250.
- [11] W. A. Khan, and I. Pop, Boundary-layer flow of a nanofluid past a stretching sheet, *International Journal of Heat and Mass Transfer* 53 (11-12) (2010) 2477-2483.
- [12] A. Noghrehabadi, R. Pourrajab, and M. Ghalambaz, Effect of partial slip boundary condition on the flow and heat transfer of nanofluids past stretching sheet prescribed constant wall temperature, *International Journal of Thermal Sciences* 54 (2012) 253-261.
- [13] A. M. Rohni, S. Ahmad, A. I. M. Ismail, and I. Pop, Flow and heat transfer over an unsteady shrinking sheet with suction in a nanofluid using Buongiorno's model, *International Communications in Heat and Mass Transfer* 43 (2013) 75-80.
- [14] A. Malvandi, F. Hedayati, D. D. Ganji, and Y. Rostamiyan, Unsteady boundary layer flow of nanofluid past a permeable stretching/shrinking sheet with convective heat transfer, *Proceedings of the Institution of Mechanical Engineers, Part C: Journal of Mechanical Engineering Science* 228 (7) (2014) 1175-1184.
- [15] M. Khan, M. Azam, and A. Alshomrani, Effects of melting and heat generation/absorption on unsteady Falkner-Skan flow of Carreau nanofluid over a wedge, *International Journal of Heat and Mass Transfer* 110 (2017) 437-446.

- [16] K. L. Hsiao, To promote radiation electrical MHD activation energy thermal extrusion manufacturing system efficiency by using Carreau-nanofluid with parameters control method, *Energy* 130 (2017) 486-499.
- [17] K. Vajravelu, and A. Hadjinicolaou, Convective heat transfer in an electrically conducting fluid at a stretching surface with uniform free stream, *International Journal of Engineering Science* 35 (12-13) (1997) 1237-1244.
- [18] A. Ishak, R. Nazar, and I. Pop, Hydromagnetic flow and heat transfer adjacent to a stretching vertical sheet, *Heat and Mass Transfer* 44 (8) (2008) 921-927.
- [19] V. N. Ganesh, B. Ganga, A. Hakeem, S. Saranya, and R. Kalaiivanan, Hydromagnetic axisymmetric slip flow along a vertical stretching cylinder with a convective boundary condition, *St Petersburg Polytechnical University Journal Physics and Mathematics* 4 (253) (2016).
- [20] Y. Q. Song, H. Waqas, K. Al-Khaled, U. Farooq, S. Gouadria, M. Imran, and Q. H. Shi, Aspects of thermal diffusivity and melting phenomenon in Carreau nanofluid flow confined by nonlinear stretching cylinder with convective Marangoni boundary constraints, *Mathematics and Computers in Simulation* 195 (2022) 138-150.
- [21] Y. J. Lim, S. Shafie, S. M. Isa, A. N. Rawi, and Q. A. Mohamad, Impact of chemical reaction, thermal radiation and porosity on free convection Carreau fluid flow towards a stretching cylinder, *Alexandria Engineering Journal* 61 (6) (2022) 4701-4717.
- [22] Y. Q. Song, H. Waqas, K. Al-Khaled, U. Farooq, S. Gouadria, M. Imran, and Q. H. Shi, Aspects of thermal diffusivity and melting phenomenon in Carreau nanofluid flow confined by nonlinear stretching cylinder with convective Marangoni

- boundary constraints, *Mathematics and Computers in Simulation* 195 (2022) 138-150.
- [23] M. Y. Malik, T. Salahuddin, A. Hussain, and S. Bilal, MHD flow of tangent hyperbolic fluid over a stretching cylinder: Using Keller box method, *Journal of Magnetism and Magnetic Materials* 395 (2015) 271-276.
- [24] S. Bilal, M. Sohail, R. Naz, and M. Y. Malik, Dynamical and optimal procedure to analyze the exhibition of physical attributes imparted by Sutterby magneto-nanofluid in Darcy medium yielded by axially stretched cylinder, *Canadian Journal of Physics* 98 (2020) 1-10.
- [25] L. D. Landau, E. M. Lifshitz, and L. P. Pitaevskii, *Magnetohydrodynamics, Electrodynamics Of Continuous Media* 8 (1984) 225-256.
- [26] R. O. Fagbenle, O. M. Amoo, A. Falana, and S. Aliu, editors. *Applications of heat, mass and fluid boundary layers*, Woodhead Publishing Limited 2020.
- [27] M. Frank, *Fluid Mechanics Fourth Edition*, McGraw-Hill, 2017.
- [28] R. R. Rangi, and N. Ahmad, Boundary Layer Flow past a Stretching Cylinder and Heat Transfer with Variable Thermal Conductivity, *Applied Mathematics* 3 (2012) 205–209.
- [29] Hashim, M. Khan, and A. S. Alshomrani, Characteristics of melting heat transfer during flow of Carreau fluid induced by a stretching cylinder, *The European Physical Journal E* 40 (2017) 1-9.
- [30] H. Waqas, U. Manzoor, T. Muhammad, and S. Hussain, Thermo-bioconvection transport of nanofluid over an inclined stretching cylinder with Cattaneo–Christov double-diffusion, *Communications in Theoretical Physics* 73 (7) (2021) 075006.